NAGW-399
IN-CAT. 75
44441
109P.

DUST-MAGNETOSPHERE INTERACTIONS

Eberhard Grün
Max-Planck-Institut für Kernphysik
Postfach 103980
6900 Heidelberg 1, F.R.G.
phone: (0)6221-516-478

Gregor E. Morfill
Max-Planck-Institut für Extraterrestrische Physik
8046 Garching, F.R.G.
phone: (0)89-3299-567

and

D. Asoka Mendis
C-014 Department of Electrical
Engineering & Computer Sciences
University of California
La Jolla, California 92093, U.S.A.
phone: (714) 452-2719

June 1983

Second draft of chapter

PLANETARY RINGS

Eds. Richard Greenberg
and André Brahic

(NASA-CR-179975) DUST-MAGNETOSPHERE INTERACTIONS (Max-Planck-Inst. fuer Kernphysik) 109 p

N87-70219
44441
Unclas
00/75 42915

Abstract

Micron-sized dust grains were identified by their light scattering characteristics in most rings of the outer planets. A multitude of interactions between the magnetospheric particles, fields and dust grains has been proposed. We review the major effects and indicate the pertinent observations. Energetic particle absorption signatures observed by Pioneer 11, Voyager 1 and 2 trace the mass concentrations of particulates in Jupiter's and Saturn's magnetospheres. Particulates which are immersed in the magnetospheric plasma and exposed to solar UV radiation will charge up to a surface potential which depends on the density and energy E_e of the plasma as well as on the concentration n_d of the dust particles. An isolated dust grain ($n_d < \lambda_D^{-3}$, λ_D = Debye length, typically 10^2-10^4cm) becomes negatively charged if the plasma electron flux exceeds the photoelectron flux ($\sim 2.5 \times 10^{10} r^{-2} cm^{-2} s^{-1}$, at the distance r in a.u. from the sun) from its surface. Its surface potential will reach $V_o \sim \frac{E_e}{e}$ (e = electronic charge). At high dust concentrations ($n_d > \lambda_D^{-3}$) the charge on the dust grains will be significantly reduced. Kinetic effects of charged dust particles arise from the interaction with the planetary magnetic field. Radial drift of dust particles is induced by systematic and stochastic charge variation and by the plasma drag. Sputtering and mutual collisions affect the sizes of grains. Electromagnetic effects are discussed which lead to the halo of Jupiter's ring, the dust distribution in Saturn's E-ring and to levitated dust in the B-ring (spokes) as well as on the moon.

Contents

I.	Introduction	1
II.	Characteristics of Jupiter's and Saturn's magnetospheres	4
III.	Physical Processes	8
III.1	Energetic particle and plasma absorption	8
III.2	Charging of dust particles	11
	a) Isolated grains	
	b) Collective effects	
III.3	Electrostatic disruption and particle levitation	21
	a) Electrostatic disruption	
	b) Electrostatic levitation and blow-off of small particles	
III.4	Sputtering	30
III.5	Plasma drag	33
	a) Direct particle drag	
	b) Distant Coulomb drag	
III.6	Mutual collisions	37
	a) High velocity collisions	
	b) Low velocity collisions	
IV.	Kinetic effects	44
IV.1	Gravito-electrodynamics	44
	a) General solution	
	b) Stability of orbits	
IV.2	Radial transport	52
	a) The adiabatic motion of charged dust grains	
	b) Systematic drift	
	c) Stochastic transport	

V.	Observations	66
V.1	Dust in the Earth's magnetosphere	67
V.2	The Jovian ring	69
V.3	Saturn's ring system	71

I. Introduction

Recent space probe measurements detected high dust concentrations in the magnetosphere of Jupiter and Saturn. Voyager 1 discovered the Jovian ring (Smith et al., 1979, see also Burns et al., 1982) after it had been suspected by Pioneer 11 data analysis (Fillius, 1976, Acuna and Ness, 1976). At Saturn Pioneer 11, Voyager 1 and 2 disclosed a number of dust phenomena (cf. Cuzzi et al. 1982). Some of them are obviously correlated with magnetosphere characteristics, e.g. the spoke phenomena in Saturn's B ring showed a periodicity with Saturn's rotation period (Porco and Danielson, 1982) which indicates a coupling of spoke activity to the planetary magnetic field.

Most dust observations were made in the inner magnetospheres where the magnetic fields and also the plasma densities are relatively high. Absorption effects of magnetospheric charged particle populations by material concentrations in Saturn's ring system were immediately evident in the observations (Simpson et al., 1980, Vogt et al., 1981). Effects of the magnetospheric particles and fields on the dust grains are more subtle and generally not easy to observe directly.

Dust-magnetosphere interactions have been studied since the first measurements of particulates in the Earth's vicinity became available. Several investigators studied the magnetospheric effects on dust concentrations in the Earth's neighborhood (Öpik 1956, Belton, 1966, Shapiro et al., 1966). These effects could not be verified by measurements because of the low dust concentration near the Earth.

Lunar observations both by remote sensing and in situ experiments showed effects of electrostatically levitated dust (Rennilson and Criswell, 1974, Severny et al., 1974, Berg et al., 1976). Recent satellite measurements

(Fechtig et al., 1979) indicated that electrostatic disruption of large fluffy meteoroids occurs in the auroral zones of the Earth's magnetosphere.

In the Jovian system Mendis and Axford (1974) proposed that dust magnetosphere interactions are responsible for the albedo variations of the Galilean satellites. From all these studies it became quite clear that only for micron-sized grains do the electromagnetic forces become important compared to the gravitational force.

Indeed, largely from observation of the relative strengths of forward and back-scattered light, it has become clear that such small (micron and sub-micron sized) grains dominate the populations of certain regions of the known planetary ring systems. These regions include the extended E-ring and the thin F- and G-rings of Saturn (cf. Cuzzi et al. 1982), as well as the extended ethereal ring of Jupiter (cf. Burns et al., 1982) with its contiguous thin inner disk and its inner lenticular halo. Also, the "near radial" spokes that are seen to rotate across the dense B-ring of Saturn and which seem to be elevated above the ring plane, are apparently composed of such small grains. Since these discoveries the number of scientists interested in the subject of dust-magnetosphere interactions is rapidly increasing.

A variety of different effects has to be considered if one studies dust-magnetosphere interactions. Plasma and energetic particles are absorbed by the particulates. Neutral atoms, molecules, ions and electrons are emitted upon the impact of energetic ions and by mutual collisions among the dust particles. Simultaneously the dust grains are eroded. Dust particles are charged by electron and ion capture from the plasma as well as by the photoelectric effect from the solar UV radiation. Electrostatic disruption of individual grains as well as mutual repulsion and levitation may occur. Momentum exchange with the plasma exerts a drag on the grains which causes a radial drift towards or away from the planet. Interaction of charged

dust particles with the planetary gravitational and magnetic fields (gravito-electrodynamics) becomes an important factor in the dynamics of highly charged small dust particles. For the description of radiation pressure effects we refer to the paper by Mignard (1982). Stochastic fluctuations of the charge state of grains causes a diffusion of small dust particles throughout the magnetosphere.

This article is intended to give an overview over the field of dust magnetosphere interactions and to show the areas of current research. In the second section we describe the environment the dust grains are exposed to: the magnetospheric particles and fields. In the following sections we discuss the physical processes (III) and kinetic effects (IV) of dust-magnetosphere interactions and in the last (V) section we discuss relevant observations in the magnetospheres of the Earth, Jupiter and Saturn and indicate the status of their interpretations.

II. Characteristic of Jupiter's and Saturn's megnetospheres.

Within a magnetosphere the magnetic field is controlled by the field inherent in the planet. Close to the planet the magnetic fields of Jupiter and Saturn can be approximated by a centered dipole (this neglects higher multipole moments which are generally small, cf. Connerney et al., 1982). The equatorial magnetic field strength is then expressed by

$$B = B_0 \cdot L^{-3} \tag{1}$$

where L is the magnetic shell parameter which corresponds (in the magnetic equatorial plane) to the distance from the center of the planet in units of the planetary radius R (with index J for Jupiter and S for Saturn). The equatorial radii are $R_J = 7.14 \times 10^9$ cm and $R_S = 6.03 \times 10^9$ cm. Spaceprobe measurements yielded values of $B_{0J} = 4.2$ gauss (Smith et al., 1974, Acuna and Ness, 1976), for Jupiter and $B_{0S} = 0.20$ gauss (Smith et al. 1980, Acuna and Ness, 1980). The same measurements showed that Jupiter's magnetic dipole axis is tilted by 10° with respect to the planetary rotation axis, with a longitude of the magnetic pole in the northern hemisphere of 230°. Saturn's dipole axis is within 1° parallel to the rotation axis. Both dipole fields have their magnetic north pole in the northern hemispheres of the planets and hence their polarities are opposite to that of the Earth's magnetic field.

The inner part of the magnetosphere out to about 10 planetary radii (the exact distance varies from planet to planet) where the magnetic field is still dipolar is called the plasmasphere. It contains plasma which rigidly rotates with the planet at a speed

$$u(r) = \Omega r \tag{2}$$

where r is the distance from the rotation axis and Ω is the rotational angular velocity. The values are $\Omega_J = 1.7585 \times 10^{-4}$ radians s^{-1} for Jupiter and 1.6378×10^{-4} radians s^{-1} for Saturn. The distance at which the angular velocity of the planet equals the circular Keplerian orbital motion (synchronous orbit)

$$\Omega = \omega_{Kep} = \sqrt{\mu / r^3} \tag{3}$$

where μ = GM with G = gravitational constant and M = mass of the planet ($\mu_J = 1.25 \times 10^{23}$ cm^3 s^{-2} and $\mu_S = 3.80 \times 10^{22}$ cm^{3}s^{-2}) is commonly referred to as the co-rotation distance r_{co}. This distance is $r_{co\ J} = 1.59 \times 10^{10}$cm (2.22 R_J) at Jupiter and $r_{co\ S} = 1.12 \times 10^{10}$cm (1.86 R_S) at Saturn.

Inside the plasmasphere the plasma density n increases towards the planet from about 1 electron cm^{-3} at L = 10 to about 10^2 cm^{-3} at L = 3 and the electron energy E_e decreases from about 100 eV to 10 eV (Frank et al. 1976, Bridge et al. 1979 and 1981). Beside this general trend there are some important local deviations (see Fig. 1). Particularly high plasma density of $n \sim 3000$ cm^{-3} is found in the Io plasma torus (Bagenal and Sullivan, 1981, Scudder et al. 1981). Especially low values ($n \approx 10^{-2}$ cm^{-2}) have been estimated by Goertz and Morfill (1982) for the region above and below Saturn's A and B rings. The composition of the ions in Jupiter's plasmasphere is mainly oxygen O^+ and sulfur S^{2+} or some combination of both ions (Frank et al. 1976, Bridge et al. 1979) and in Saturn's plasmasphere oxygen O^+ has been identified (Bridge et al. 1981, 1982).

Outside the plasmasphere the magnetic dipole field is distorted by ring currents carried by the plasma. The densities are low 10^{-2} cm$^{-3} \leq n \leq 1$ cm^{-2} but the energies may be well above 1keV (Bridge et al. 1979, and 1981).

Beside this low energy plasma a second but distinctly different charged particle population also occupies the inner part of the magnetosphere. This is the high energy (MeV) particle population of the radiation belts. The fluxes may reach 10^7 cm^{-2} s^{-1} in the regions of highest intensities (Fillius, 1976, Fillius et al. 1980).

From the plasma density and the electron energy E_e other important parameters like the Debye length λ_D (shielding length in the plasma)

$$\lambda_D = \sqrt{\frac{E_e}{4\pi e^2 n_e}} \tag{4}$$

or

$$\lambda_D(\mathrm{cm}) = 740 \sqrt{\frac{E_e(\mathrm{eV})}{n_e(\mathrm{cm}^{-3})}} \tag{4a}$$

and the electron flux

$$\phi_e = n_e \sqrt{\frac{2E_e}{m_e}} \tag{5}$$

can be derived, where the electron density is n_e, e is the electronic charge and m_e is the electron mass. These quantities are also shown in Fig. 1. The Debye length varies from 10^2 to 10^4 cm in the inner magnetosphere and the electron flux ranges from 10^6 to 10^{11} $\mathrm{cm}^{-2}\mathrm{s}^{-1}$.

For comparison we also show the flux of photoelectrons released from a metal surface which is illuminated by the sun at the distance of Jupiter (5.2 AU) and Saturn (9.5 AU). The flux of photoelectrons from such a surface at the Earth's distance (1 AU) is 2.5×10^{10} $\mathrm{cm}^{-2}\mathrm{s}$ (Wyatt 1969). This number is based on the solar UV flux measurement by Hinteregger (1964) and on measurements of the wavelength dependent photoyield. Feuerbacher and Fitton (1972) extended this work to other materials including non-conducting materials like silica and indium oxide and carbonaceous materials like Aquadag, vitreous carbon and graphite. Graphite showed the lowest yield, approximately one order of magnitude lower than the photoyield of metals. The yields of indium oxide and silica were intermediate. Therefore the photoelectronic flux from natural dielectrics like ices and stones may be somewhat lower than that from metals. The comparison of the fluxes shows that in the inner plasmaspheres of Jupiter and Saturn

the plasmaelectron flux exceeds the photoelectron flux by far except in the regions of the A and B rings of Saturn.

III. Physical Processes

III.1 Energetic particle and plasma absorption

Both cold (eV) plasma and energetic (MeV) particles coexist in inner magnetospheres. The energetic particle population which consists mainly of electrons and protons is trapped by the planetary magnetic field. There is a hierarchy of motion represented by the time scales involved (the times shown are valid for 1 MeV protons in Jupiter's and Saturn's magnetospheres, respectively, at L = 3) of a trapped particle in a magnetic dipole field: 1. gyration about its guiding field line ($2x10^{-3}s$, $5x10^{-2}s$), 2. the bounce motion (33s, 28s) due to mirroring in the stronger magnetic field regions closer to the poles of the planet and 3. a longitudinal drift motion ($2x10^{6}s$, $6x10^{4}s$).

Both spatial and temporal inhomogeneities in the magnetic and the related electric fields which are comparable to the gyroradius or gyroperiod will introduce non-adiabatic particle orbits which in consequence will cause a radial diffusion of the trapped particles (cf. Schulz and Lanzerotti, 1974). Fig. 2 (curve a) shows the distribution of the phase space density of energetic particles as a function of the magnetic shell parameter L. The phase space has been specified at an outer boundary (L_4) and is assumed to be zero at an inner boundary (L_0). Between these boundaries no local sources or sinks have been assumed. The phase space density declines monotonically as L decreases from L_4 inward and exhibits no maxima or minima.

If there is a partially absorbing ring of particulates in that region of space then the number of charged particles is reduced in the tubes of magnetic lines of force passing through the ring. The local phase space density of energetic particles is reduced in the range of the ring between L_1 and L_3 (Fig. 2, curve b). Since there is no source assumed in that region there is no maximum. The same "macro-signature" (curve b) is seen for a satellite orbiting in the radius interval between L_1 and L_3 if one measures

the time-average phase space density. Close to a satellite, however, the total depletion of energetic particles due to the absorption of all particles from a tube of magnetic field lines which intersects the satellite can be observed. The particle shadow of a satellite for a particular class of particles either precedes or follows, depending on the relative drift motion, the satellite in its orbital motion and is gradually filled in (as a function of longitude ahead of or behind the satellite) by radial diffusion. Such a time-dependent signature that is localized in longitude is called "micro-signature" (Fig. 2, curve c). The time-averaged or longitudinally-averaged effect on the radial distribution of trapped particles is the above described macro-signature of a longitudinally uniform distribution of dispersed particulate matter in the form of a ring. A longitudinally localized distribution of particulates can masquerade as a satellite and would be difficult to distinguish from a satellite by the particle absorption technique.

The power of this technique for the identification of concentrations of particulates has been demonstrated by the Pioneer 11, Voyager 1 and 2 measurements at Jupiter's and Saturn's rings. (Fillius 1976, Goertz and Thomson 1979, Van Allen et al. 1980 a,b,c, Van Allen, 1982). Energetic particle absorption signatures near Saturn's G ring repored by Van Allen et al. (1980b) were interpreted as a mass density per unit area normal to the ring plane of $\gtrsim 7\times10^{-9}$ g/cm^{-2} (Van Allen personal communication, reported by Gurnett et al. 1982). In the region of the F ring Van Allen et al. (1980a) reported three individual micro-signatures which were interpreted by Van Allen (1982) as three nearby satellites or longitudinally-localized distributions of dispersed particulate matter at radial distances of 141,179 $\pm$ 100 km, 140,630 $\pm$ 80 km and 140,150 $\pm$ 80 km. For comparison the (elliptical) F ring has been optically identified at a mean distance of 140,300 km from Saturn's center.

Morfill et al. (1980d) suggest that also in the Jovian system outside the optically visible ring a concentration of small dust particles leads to significant losses throughout the inner magnetosphere which are in agreement with the available energetic electron measurements (Van Allen, 1977).

Also thermal plasma is affected by the absorption by a tenuous ring. Voyager 1 and 2 observations of the electron distribution showed a depletion of higher energy electrons (above 700 eV) by Saturn's E ring (Sittler et al. 1981). The lower energy electrons are not affected because their bounce frequency and collision frequency which are proportional to the particle energy are lower and hence their absorption rate is reduced. Sittler et al. (1981) showed that the E ring extends out to about 9 R_S and is not symmetrical about Saturn. They also found some absorption signatures between 15 and 17 R_S and outside 20 R_S.

III.2 Charging of dust particles

Dust particles which are immersed in a plasma will be hit by electrons and ions. These electrons and ions will stick to the dust grain and change its charge state until the flux of positive charges onto the surface equals the flux of negative charges. If there are other currents of charged particles to and from the surface like photoelectron and secondary particle emission they also have to be taken into account. Charge equilibrium is reached when the sum of all currents equals zero. Two cases can be distinguished: first, there is only one isolated particle within a sphere of the radius of the Debye length λ_D and second there are many particles within a Debye sphere and the electric fields of neighbouring particles overlap. We shall begin with the case of

a) Isolated grains

We want to calculate the particle's surface charge and its variation with time when it is immersed in a plasma and irradiated by solar UV radiation. The plasma has a density $n = n_e = n_i$ and a thermal electron energy E_e and ion energy E_i. We shall assume that the thermal electron and ion velocities are much greater than the dust grain velocity so that we may consider the particle at rest with respect to the plasma. In a Maxwellian plasma with electron temperature T_e and ion temperature T_i (or thermal energies $E_e = kT_e$ and $E_i = kT_i$, respectively, where k is the Boltzmann constant) the rate of incidence of electrons on a grain of radius s and of (positive) charge N e (e = electronic charge) results in a charging rate of

$$\left.\frac{dN}{dt}\right|_e = -\pi s^2 \alpha_e \, n_e \, c_e \exp\left(Ve/kT_e\right) \qquad (6)$$

where α_e is the "sticking efficiency" of electrons (~ 1) to the grain

and $V = Ne/s$ is the potential of a (spherical) particle which has the surface charge $q = Ne$ (number of electrons $N = 700\ V\ s_\mu$, with V in volts and grain radius s_μ in μm). The rate at which positive ions are incident leads to a gain in (positive) charge at a rate given by

$$\left.\frac{dN}{dt}\right|_i = \pi s^2 \alpha_i\ n_i\ c_i \exp\left(-eV/kT_i\right). \qquad (7)$$

α_i is the "sticking efficiency" of ions (≈ 1) and c_e and c_i are the thermal velocitites of electrons and ions, respectively, in a Maxwellian plasma

$$c_e = \sqrt{\frac{2kT_e}{m_e}} \qquad \text{and} \qquad c_i = \sqrt{\frac{2kT_i}{m_i}} \qquad (8)$$

The rate of increase of (positive) charge on the grain due to photoemission is (Wyatt, 1969):

$$\left.\frac{dN}{dt}\right|_{pe} = \pi s^2\ K\ f\ (V) \qquad (9)$$

where we can represent f(V) approximately by

$$f(V) = \begin{cases} 1 & \text{if } V \leq 0 \\ e^{-V/V^*} & \text{if } V > 0 \end{cases} \qquad (10)$$

Wyatt (1964) estimates a yield $K = 2.5\times10^{10} \left(\frac{R_o}{r}\right)^2$ photoelectrons per cm² and second in the solar UV spectrum at $r = R_o = 1$ AU for a metal target. This number may be reduced by a factor of 0.1 for dielectrics (Feuerbacher and Fitton, 1972). The constant V^* depends on the mean kinetic escape energy which the photoelectrons have and is of the order of $V^* = 3$ V.

The equilibrium potential V_o is then found by setting

$$\left.\frac{dN}{dt}\right|_e + \left.\frac{dN}{dt}\right|_i + \left.\frac{dN}{dt}\right|_{pe} = 0 \qquad (11)$$

If the photoelectron flux dominates (cf. Fig. 1) the equilibrium charge will be positive and the exp(-V/V*) factor automatically ensures small potentials of the order $V_o \sim V^*$. The charge on the dust particle is given by

$$q = \frac{sV_o}{300} \quad . \qquad (12)$$

where q is in e.s.u., s in cm and V_o in volts.

This situation applies to interplanetary space (Rhee, 1967, Wyatt 1964) and to regions where the plasma flux is low (e.g. above Saturn's A and B rings). In the dense plasma regions of the magnetospheres, the thermal electron flux exceeds all other fluxes on a grain at potential V = 0. In the case where plasma electron flux and photoelectron flux are the main fluxes, the equilibrium potential V_o is given approximately by

$$eV_o \approx - E_e \ln \frac{n_e c_e}{K} , \qquad (13)$$

If photoelectron flux is negligible compared to the plasma electron flux (i.e. $n_e c_e >> K$) then balance is achieved by (6) and (7) and we get

$$eV_o \approx -E_e \frac{1}{2} \ln \left(\frac{E_e m_i}{E_i m_e}\right) / \left(1 + \frac{E_e}{E_i}\right). \qquad (14)$$

In other words, if $n_e c_e < K$ (by a factor of 2 or more), the equilibrium potential is V_o = order of $(\frac{E_e}{e})$ and is negative.

The charging time constant τ can be obtained from Fig. 3 (after Johnson et al., 1980) for the case where plasma fluxes dominate. For given plasma energies,

E_e and E_i the product τns is obtained, e.g. if $E_e = E_i = 100$ eV, $\tau ns = 0.3$, for a plasma density $n = 10\ cm^{-3}$ and $s = 10^{-4}$ cm a charging time constant of $\tau = 30$ s is calculated. The surface potential V of the dust grain varies with time as

$$V = V_o\ (1 - g \exp\ (-t/\tau)) \qquad (15)$$

where the initial charge is $V(t = 0) = V_o(1-g)$. These short time scales show that the potential on the grain surface follows variations of the plasma parameters (n_e, E_e) which have comparable or longer time scales. Therefore the charge state of a dust grain is determined by the local plasma conditions.

The negative equilibrium potential may be altered towards less negative values by several effects. If the dust particle is in motion relative to the plasma with a speed $w = v-u$ (v = orbital speed of the dust particle and u is the co-rotational speed of the plasma) which becomes comparable with the thermal speed of the ions or even with that of the electrons, then the currents onto the dust grain are enhanced. Typical relative speed range from $w = 0$ at the co-rotation distance to several 100 km/s in the outer plasmasphere. The thermal speed of 100 eV electrons is 6×10^3 km/s whereas the thermal speed of oxygen ions of the same energy is 35 km/s. With respect to the electrons, the dust particles move with subsonic speed in all regions of the magnetosphere. But with respect to the ions the motion is supersonic in the outer parts of the plasmasphere. Therefore the ion flux onto the dust grain is enhanced and hence the negative equilibrium potential V_o is reduced. A full treatment of this case is given by Wyatt (1969) and Mendis (1981).

At plasma energies above 10 eV secondary emission from solid particles becomes important and causes a reduction of the negative equilibrium potential . At plasma energies above 100 eV the yield of secondary electrons may become larger than 1 for some materials and the charging effect of the impacting electrons reverses because more electrons are released than picked up. The equilibrium potential will then become $\sim$ 10 V positive since the energies of the secondary electrons are typically 10 eV. This effect has been discussed in more detail by Meyer-Vernet (1982).

b) Collective effects

An ensemble of dust particles embedded in a plasma is, of course, not necessarily described by the single, isolated particle approach used previously. The question is, when are "collective" effects important. By "collective" we mean here not the mass, momentum and energy interchanges which occur in a mass loaded plasma, but the interactions between neighboring particles and the resultant influences on the plasma, and, in turn, the backreaction on the dust particles.

"Collective" effects are important, when the plasma relaxation time scales and natural length scales become larger than the determining time and length scales of the dust distribution.

One important process is the redistribution of the plasma in the presence of a foreign point charge. The associated length scale is the Debye length, λ_D, the time scale is given approximately by λ_D/c_e, where c_e is the electron thermal velocity. The redistribution of the plasma implies that the foreign point charge is shielded from the rest of the system outside a distance of a few λ_D. If the mean separation between dust particles, $d = n_d^{-1/3}$ (where n_d is the spatial density of the dust particles), is smaller than λ_D, neighboring dust particles are not shielded and isolated from each other - they begin to act like a solid dielectric. For a flat extended ring, this implies that the ring particle surface potential must be calculated as if it were a flat plate. Needless to say, the influence of the neighboring particles, then simply lead to a reduction in the total ring surface charge. As shown by Morfill (1982a,b)

and Goertz and Morfill (1982) for the case of Saturn, the ring potential can be calculated from

$$V_R = V^* \{ \ln \frac{K}{2K_I} (1-\exp-\tau_R) \} \qquad (16)$$

with the workfunction for ice $V^* = 3$ V, the photoelectron yield for ice at Saturn $K = 2.5\times10^7 cm^{-2}s^{-1}$ and the photoelectron-flux from the ionosphere $K_I = 2.5\times10^5 cm^{-2}s^{-1}$. This yields values for the ring potential $V_R \cong +10$ volts for optical depth $\tau_R = 1$ and $V_R \cong +4.7$ volts for optical depth $\tau_R = 0.1$. The corresponding surface charge density is

$$\sigma = V_R/4\pi\lambda_D \qquad (17)$$

Again for Saturn's rings, this yields $\sigma \cong 500$ electrons/cm^2 ($\tau_R \cong 1$). Ring particles with a systematic charge greater than +e (electron charge) must have radii greater than ~ 0.05 cm. Smaller particles have only statistically fluctuating charges. We will see that only micron-sized particles (or sub-micron) are at all likely to be electromagnetically affected. If these particles carry essentially no charge, as seems indicated by these considerations, then it must be concluded that, on average, elctromagnetic processes are unimportant in sufficiently dense planetary rings. They may be of interest for ring "halos", if these consist of dust grains which are sufficiently small and not too abundant. If the "halo" was for some reason, too dense, it would shield itself electrically, the perturbing electromagnetic forces would be turned off and the dynamical evolution would be governed by dust-dust collisions, finally leading to a flattened ring, unless it is continually replenished.

Of interest is perhaps also the fact that small, practically neutral, ring particles fluctuate from -1, 0, +1 e over time scales given by the solar UV flux and its photoionisation efficiency. At Saturn, this time scale is

$$\tau_{pe} = 1/(\pi s^2 K) \sim 1.3/s_\mu^2 \text{ sec} \tag{18}$$

where s_μ is the particle radius in microns. The material was assumed to be ice. Furthermore, if the electron energies are $\sim$ few eV (and thus $c_e \approx 10^8$ cm/sec), any plasma density in excess of ~ 0.25 cm^{-3} suffices to charge isolated dust particles in Saturn's magnetosphere negatively. The Debye length is then

$$\lambda_D \cong 10^3/\sqrt{n_e} \text{ cm} \tag{19}$$

and the time scale for plasma readjustment is

$$\tau_d \equiv \lambda_D/c_e \cong 10^{-5}/\sqrt{n_e} \text{ sec} \tag{20}$$

This time scale is much faster than any time scale involving dust grains (such as charge fluctuation time scale, time scale involving translational motion, collision time scales, momentum exchange time etc.). Hence no higher order corrections are ever required in the situations discussed here.

Let us consider, quite generally, a dust ring with normal optical depth, τ , mean particle size s and scale height h. The dust particle number density is then

$$n = \tau/\pi s^2 h \tag{21}$$

and the mean separation between dust particles is

$$d = n^{-1/3}. \tag{22}$$

From (19) and (22) we define the parameter η:

$$\eta \equiv \frac{\lambda_D}{d} \sim \frac{3.2\times10^5}{\sqrt{n_e}} \left(\frac{\tau}{h}\right)^{1/3} \tag{23}$$

where h is the scale height measured in cm, and s has been set equal to 1 micron. In Table 1 we list estimates of η for some specific rings (note that we have always used $c_e = 10^8$ cm/sec - some plasma environments may be somewhat "hotter").

Table 1: Electrical conditions in planetary rings

Ring	plasma density (cm^{-3})	normal optical depth	scale height (km)	η
Jupiter ring	< 100	$\sim 10^{-5}$	< 30	> 5
Jupiter halo	$\sim$ 100	$\sim 10^{-6}$	10^4	0.5
E ring	$\gtrsim$ 10	10^{-6}	10^4-10^5	0.5-1
G ring	$\sim$ 10	10^{-6}	10^3	2
F ring	< 10	$\sim$ 0.1	< 1	> 10^3
A and B ring	$\sim 10^{-2}$	1	1	$\sim 10^5$
Spokes region	$\sim$ 100	0.1	$\sim$ 30	$\sim$100

As can be seen from the table, the only clearcut case where dust particles are isolated, are the Jovian ring halo and the E ring of Saturn. All other systems (at least when they are fully evolved, e.g. in the case of the "spokes") must be regarded as "collective", in the sense defined earlier.

This implies that electromagnetic perturbations are unlikely to be important for most ring phenomena - except the E ring, Jupiter's ring halo and, perhaps, disc and G ring.

III.3 Electrostatic disruption and particle levitation

A consequence of the electrical charging of dust particles is their possible bursting due to the electrostatic stresses and the mutual repulsion of homogeneously charged grains. If one particle is much larger than the other and if the repulsion is counteracted by the gravitational attraction then this situation is commonly referred to as electrostatic levitation (see below).

a) Electrostatic disruption

This mechanism was first described for interplanetary meteoroids by Öpik (1956). Electrostatic disruption of charged dust particles occurs if the tensile strength F_t of the particle in dynes per square centimeter is exceeded by the electrostatic repulsive force acting on a sphere of radius s(cm) at a surface potential V_o(V):

$$F_t < 8.85 \times 10^{-7} V_o^2/s^2 \qquad (24)$$

The relevant tensile strength (and the corresponding maximum surface field strength V_o/s) is $\sim 10^4$ dyn cm^{-2} (10^5 V/cm) for fluffy aggregates, 10^6 to 10^8 dyn cm^{-2} (10^6 to 10^7 V/cm) for ice, 10^7 to 10^9 dyn cm^{-2} (3×10^6 to 3×10^7 V/cm) for silicates, $\sim 7\times10^9$ dyn cm^{-2} (9×10^7 V/cm) for glass and $\sim 2\times10^{10}$ dyn cm^{-2} (1.5×10^8 V/cm) for metals (Öpik, 1956; Rhee 1976; Pollack et al. 1979, Burns et al. 1980). Figure 4 shows lines of constant tensile strength (i.e. field strength) as a function of particle radius and surface potential.

Micron- and submicron-sized particles have increased strength because they may consist of individual crystals. For these particles the maximum field strength attainable at the surface is limited by ion field emission in the case of positive grain charge or by electron field emission in case of negative grain charge. The maximum field strength is then $\sim 5 \times 10^8$ and $\sim 10^7$ V/cm for ion and electron field emission, respectively (Müller 1956). Charging of spherical dust particles made of carbon, glass and metals in the laboratory resulted in surface field strengths which were within a factor of 5 of the ion field emission limit without destroying the dust particles (Vedder 1963; Friichtenicht 1964; Fechtig et al 1978). However, dust particles in planetary rings may be more friable than generally undamaged laboratory specimens from collisions among ring members (Burns et al 1980, Hörz et al 1975) and from radiation damage (Mukai 1980; Smoluchowski 1980). Both effects enhance flaw densities and thereby weaken grains.

While Öpik (1956) calculated the electrostatic pressure for spherical grains, a more general derivation for prolate and oblate spheroids is given by Hill and Mendis (1981b). Another more general description of electrostatic bursting is obtained for particles with rough surfaces if the dimension s appearing in (24) is that of a typical asperity, not that of a whole grain. Since any roughness is usually much smaller than the grain itself, the stresses acting on surface elements are considerably higher than (24) provides. Such surface bumps will first be eroded away and the grain will become more spherical. The final result will be one of two things: If the tensile strength of the

grain is sufficiently, large the end chipping process will eventually cease. Otherwise, it will continue chipping off until it becomes spherical, at which time it will explode *in toto.*

b) Electrostatic levitation and blow-off of small particles

In this paragraph we want to study the combined effect of electrostatic repulsion and gravitational attraction of spherical particles with radii s_o and s, where $s_o >> s$. The small particle may be one which is electrostatically chipped off from the larger one or which inelastically collided with the larger one and got stuck due to gravitational attraction when there was less electrostatic repulsion between the particles. The effects of spinning particles and of particles within the Roche limit will be discussed (at the end of this paragraph). In a plasma with Debye length λ_D the large particle will be charged to the surface potential V_o which depends on the plasma conditions and the solar UV flux. The electric potential U at a point $r (r > s_o)$ from the center of the large particle is given by

$$U = \frac{V_o s_o}{r} e^{-\frac{r-s_o}{\lambda_D}} \tag{25}$$

and the electric field strength $\vec{\mathcal{E}}$ is

$$|\vec{\mathcal{E}}| = V_o \frac{s_o(\lambda_D + r)}{r^2 \lambda_D} e^{-\frac{r-s_o}{\lambda_D}} \tag{26}$$

The small dust grain lying on the surface would acquire a charge q (we will assume $s \ll \lambda_D$). This charge is proportional to its projected surface area, as was first pointed out by Singer and Walker (1962):

$$q = \pi s^2 \sigma_o = \pi s^2 \frac{\mathcal{E}_o}{4\pi} \tag{27}$$

where σ_o is the surface charge density on the large particles and $\mathcal{E}_o$ is the surface field strength. Setting $r = s_o$ and substituting (26) in (27) yields

$$q = \frac{1}{4} s^2 V_o \frac{\lambda_D + s_o}{\lambda_D \cdot s_o} \tag{28}$$

Notice that this charge is much smaller than the charge ($q = sV_o$) that would be acquired by the grain if it was at a potential V_o in free space. The number of electronic charges N on such a grain is given by

$$N = \frac{q}{e} = 1.74 \times 10^{-4} \; s_\mu^2 \; V_o \frac{\lambda_D + s_o}{\lambda_D \cdot s_o} \tag{29}$$

with s_μ in μm, V_o in volts and λ_D and s_o in meters. The value N for a micron-sized grain lying on a $s_o = 1$ m particle at $V_o = 10$ V and $\lambda_D = 10$ m is 1.9×10^{-3}. Obviously a grain cannot have a fractional electronic charge, and the proper interpretation of this number is that the net charge of N^{-1} small grains lying on the surface of the bigger one is unit charge, i.e. some of them are positively charged due to the loss of

a photoelectron, some are negatively charged by the capture of a plasma electron and many are uncharged (we assumed zero conductivity through the large particle).

As soon as the small grain leaves the larger particle it may acquire its full free space charge $N = 700\ V_o s_\mu$. Therefore we will discuss in the following sections both extreme cases $N = 1$ and $N = 700\ V_o s_\mu$. The condition that the small grain escapes the gravitational field of the larger particle is that the energy E_{el} gained from the electric field of the larger particle exceeds the gravitational energy E_{gr}: $E_{el} > E_{gr}$ or

$$N_e V_o > G\ M_o\ m/s_o \tag{30}$$

where G is the gravitational constant and M_o is the mass of the large particle. If both particles are spherical and have densities of 1 g/cm^3 then the critical grain radius $s_{\mu c}$ (μm) is given by

$$s_{\mu c} = 5.1 \left(\frac{V_o}{s_o^2}\right)^{1/3} \quad \text{for } N = 1 \tag{31a}$$

and

$$s_{\mu c} = 310\ \frac{V_o}{s_o} \quad \text{for } N = 700\ V_o s_\mu \tag{31b}$$

with V_o in volts and s_o in meters. A particle of radius $s_\mu < s_{\mu c}$ will escape the gravitational attraction of the larger particle. This dependence is also shown in Fig. 4 for V_o = 10 Volts, s_o = 1.8 m (which is a typical particle size in

Saturn's B ring) and for both extreme charge states. Fig. 5 shows the dependence of the critical radius from the radius of the large particle at V_o = 10 volts.

If the large particle is much larger than the Debye length λ_D then the small grain may be levitated without being able to escape from the gravitational field of the large particle (e.g. a satellite). This effect is described by comparing the forces acting on the small grain. The electric force of repulsion, F_{el}, on a grain carrying the charge Ne at the surface of the larger particle, is given by

$$F_{el} = Ne\ V_o \frac{\lambda_D + s_o}{\lambda_D \cdot s_o} \approx 1.60 \times 10^{-14}\ N \cdot V_o \frac{\lambda_D + s_o}{\lambda_D \cdot s_o} \qquad (32)$$

with the same units as in (29) and F_{el} in dynes.

The gravitational force F_{gr} on a grain of radius s lying on a larger potential of radius s_o is given by

$$F_{gr} = \frac{4}{3}\pi s^3 \rho \cdot \frac{4}{3}\pi s_o^3 \rho_o \frac{G}{(s+s_o)^2} \qquad (33)$$

where ρ and ρ_o are the densities of the small and the large particle, respectively. With $\rho = \rho_o = 1\ g/cm^3$ and $s_o >> s$ we get

$$F_{gr} \approx 1.17 \times 10^{-16}\ s_\mu^3 \cdot s_o \qquad (34)$$

in dynes. The condition for such a grain to leave the surface is $F_{el} > F_{gr}$. This gives a critical grain radius

$$s_{\mu c}' = 5.1 \times \left(V_o \frac{\lambda_D + s_o}{\lambda_D \cdot s_o} \right)^{1/3} \quad \text{for } N = 1 \tag{35a}$$

and

$$s_{\mu c}' = 310 \times \frac{V_o}{s_o} \left(\frac{\lambda_D + s_o}{\lambda_D} \right)^{1/2} \quad \text{for } N = 700\ V_o s_\mu \tag{35b}$$

Both relations are displayed in Fig. 5 for $V_o = 10$ volts and a typical Debye length of $\lambda_D = 10$ m. If $s_o > \lambda_D$ small particles may be levitated although they are not able to escape from the gravitational attraction of the large particle. This effect will lead to a halo of small particles around the bigger one at a height of the order of λ_D.

A spin of the large particle with a period T leads to a modification of the attractive force (33). The effective gravitational force F_{gr}' on a small grain lying at latitude λ (i.e. angle from the rotational equator) on a large particle is given by

$$F_{gr}' = F_{gr} \left(1 - \frac{3\pi \cos^2 \lambda}{G \rho_o T^2}\right) \tag{36}$$

At the critical spin period

$$T_c = \left(\frac{3\pi \cos^2 \lambda'}{G \rho_o} \right)^{1/2} \tag{37}$$

small grains are only gravitationally bound to the surface of the large particle at latitudes $\lambda > \lambda'$. For a density $\rho_o = 1$ g/cm^3 small particles will not stick (by gravitation) to the

equatorial regions of the large particle if its rotation period is shorter than $T_{c'}$ $(\lambda' = 0) = 1.19 \times 10^4$ s ≈ 3 h 18 min.

Another modification of the attractive forces comes from the fact that both particles move in the gravitational field of the planet. The gravitational field of a particle of radius s_o is altered by the tidal forces exerted by the planet with radius R. Qualitatively, the gravitational attraction at the sub- and anti-planet points of the spherical particle's surface is weakened whereas the attraction is increased at the poles (with respect to the orbit plane) of the particles. At the leading and trailing edges the gravitational force of the particle remains approximately unaltered. The Roche limit is given by

$$r_L = \alpha(\rho/\rho_o)^{1/3} R \qquad (38)$$

where ρ is the density of the planet ($\rho_J = 1.33$ g/cm^3, $\rho_S = 0.66$ g/cm^3), ρ_o is the density of the particle and α is a factor describing the shape of the particle ($\alpha = 1.44$ for a spherical particle and $\alpha = 2.46$ for a particle relaxed to hydrostatic equilibrium, see Dermott et al. 1979 and Dermott 1982).

Most of the rings of Jupiter, Saturn and Uranus are located close to or even inside the Roche Limit (Dermott et al. 1980). Inside the Roche limit for spherical bodies only particles with finite tensile strength can exist. Therefore loose dust grains lying at the surface of a larger particle will be lost from the caps that are closest to and furthest from the planet. Only in the polar regions a dust coverage (regolith) may exist

even inside the Roche limit. For a more detailed discussion of the effects occurring near and inside the Roche limit see Dobrovolskis and Burns (1980), Davis et al. (1981). The additional effect of electric charging, i.e. electrostatic repulsion, will clear larger areas around the sub- and anti-planet points from the dust. Therefore close to and inside the Roche limit an increase of the surface potential of particles, due to changes in the plasma parameters and the UV illumination, will lead to the levitation and escape of dust grain which otherwise would stick to the surface of larger particles.

III.4 Sputtering

The bombardment of solid particles by the intense flux of magnetospheric ions at energies above several tens of eV releases atoms, molecules and ions from the target. The sputtering yield S (i.e., the number of secondary particles per incident ion) depends strongly both on the target material and the energy and atomic number of the incident ions (for a review see, e.g., Carter and Colligon, 1968, or Oechsner, 1975). Sputtering yields S are determined by laboratory simulation and have been reported by Wehner et al. (1963) for astrophysically important systems like hydrogen and helium ions onto metal and stone targets in the energy range of 1 to 20 KeV. For protons typical values of S_p = 0.01 to 0.04 and for α-particles values of S_α = 0.1 to 0.4 have been found. For higher primary ion masses the sputtering yield passes through a maximum of the order of S = 10 when the mass of the primary ion is similar to that of the substrate atom (Wechsung, 1977). At higher energies the sputtering yield increases. Recently Brown et al. (1978 and 1980) reported the sputtering yield of ice bombarded by hydrogen, helium, carbon and oxygen ions at energies at 1.5 MeV. Hydrogen showed a yield of S_p = 0.2 to 0.4, helium S_{He^+} = 10, and carbon and oxygen $S_{C^+,O^+} \sim 500$. Sputtering is a source for magnetospheric atoms and ions. This effect is being discussed as an important source for the heavy ions in the Io torus (see Matson et al., 1974) and in Saturn's plasma sheet (cf. Cheng et al., 1982).

On the other hand sputtering erodes particulate matter. The sputter erosion of lunar rocks by solar wind ions has been determined both theoretically and experimentally (for a review see, e.g., Ashworth, 1978). The best value for the sputter rate on the lunar surface is 1.6×10^{-17} cm s^{-1}. This value refers to a flux of solar wind ions (roughly 95% protons and 5% α-particles) of $\phi_{sw} \sim 2 \times 10^8 cm^{-2} s^{-1}$ at a speed of ∿ 400 km/s.

Lanzerotti et al. (1978) studied the sputter erosion of the icy surfaces of the Galilean satellites Europa, Ganymede and Callisto by high energy protons (E > 100 keV) of the Jovian radiation belt. Their estimated sputter rates of water ice are presented in Table 2. Matson et al. (1974) estimated the sputter rate at Io from the observed sodium cloud to be 1.5×10^{-15} 1.5×10^{-14} cm s^{-1}. An upper limit of the sputter rate at Io of 8×10^{-14} cm s^{-1} has been determined by Haff et al. (1979). They considered the heavy ion impact on ice at a velocity of 50 km/s which corresponds to an energy of 300 eV for ions of atomic mass 20. This sputter mechanism is most effective in the densest parts of Io's plasma torus.

The shortest lifetimes τ_s with respect to sputtering (order of 10 years) for 1 μm ice particles are found in the Io torus and between Io and Europa. Silicate particles, however, would be expected to have about 10 times longer lifetimes than ice particles.

In the inner (4.5 - 8 R_s) Saturnian system Cheng et al. (1982) calculate that high energy sputtering by protons above 50 keV at a flux of $\sim 10^7$ $cm^{-2}s^{-1}$ yield a water ice erosion rate of 3×10^{-16} cm s^{-1}. This rate may also apply to the inner satellites Mimas (3.1 R_s) and Enceladus (4.0 R_s) since there the observed high energy proton flux is comparable to that further out (Krimigis et al., 1981, 1982). Morfill et al. (1982b) consider the sputtering by low energy heavy plasma ions. Co-rotational energies of oxygen ions in the E-ring region (3.5 to 9 R_s) range from 50 to 500 eV. Sputtering yields from low energy heavy ions impact are S = 1 to 10 secondary particles per ion. This effect becomes dominant over the high energy ion sputtering in the inner Saturnian magnetosphere because the high energy particle flux (above 100 keV) is much reduced compared to that in the Jovian system. Ice particle lifetimes range from 100 to 10^4 years in the region of the E ring.

Table 2: Erosion rates due to ion sputtering and life times of 1 μm ice particles

a) Jovian System

Satellite	Distance (R_J)	Erosion rate ($cm\ s^{-1}$)	τ_s for 1 μm (yr)	References
Io	5.90	1.5×10^{-15} - 1.5×10^{-14}	2×10^3 - 2×10^2	Matson et a. (1974)
		< 8×10^{-14}	> 40	Haff et al. (1979)
Europa	9.40	10^{-14} - 3×10^{-12}	3×10^2 - 1	Lanzerotti et al. (1979)
Ganymede	14.99	10^{-15} - 3×10^{-13}	3×10^3 - 10	"
Callisto	26.33	6×10^{-18} - 2×10^{-15}	5×10^5 - 2×10^3	"

b) Saturnian System

Mimas	3.12	3×10^{-16}	10^4	Cheng et al. (1982)
Enceladus	3.98	3×10^{-16}	10^4	"
		8×10^{-16}	6×10^3	Morfill et al (1982b)
Tethys	4.92	2×10^{-14}	1.5×10^2	"
Dione	6.28	3×10^{-14}	1.5×10^2	"
Rhea	8.75	2×10^{-15}	2×10^3	"

III.5 Plasma drag

Dust grains travelling through a plasma will exchange momentum with the plasma particles to exert a drag on the grain. This drag force is a function of the relative speed of the dust grain with respect to the plasma. At the co-rotation distance r_{co} no drag force is exerted because the grain is at rest with respect to the plasma frame of reference. Inside the co-rotation distance the plasma drag decelerates the orbital speed of the grain and hence the orbit decays towards the planet. Outside the co-rotation distance, however, the plasma drag accelerates the grain's orbital speed and therefore the orbit expands and the particles are pushed towards larger distances from the planet. This effect competes with the drag force exerted by the radiation pressure which causes the grains to lose orbital energy (cf. Mignard, 1982).

a) Direct particle drag

In this case we assume that the bulk energy of the plasma ions is much greater than the potential of the surface charge. The grain moves with a velocity $\vec{w} = \vec{v}-\vec{u}_p$ with respect to the plasma, where $\vec{v}$ is the orbital speed of the dust particle and $\vec{u}_p = r\Omega\hat{\phi}$ is the co-rotational bulk speed of the plasma at the distance r from the rotation axis, with the angular velocity Ω and $\hat{\phi}$ is an azimuthal unit vector.

Then we can write for the force acting on the dust particle

$$F_D = \int_{-\infty}^{\infty} n(u)\, \pi\, s^2\, |u-w|\, m_i\, (u-w)\, du \qquad (39)$$

here u is the thermal ion speed, and m_i is the mass of a plasma ion. The

direction of the drag force is antiparallel to $\vec{w}$. It is assumed that the distribution function for the plasma is Maxwellian, i.e.,

$$n(u) = n_i \frac{1}{\sqrt{\pi}\, c_i} \quad \exp\left(u^2/c_i^2\right) \tag{40}$$

Substituting (40) into (39) yields, for direct collisions between plasma ions and dust particles,

$$F_D = - n_i \cdot \pi s^2 m_i c_i^2 \left\{ \frac{w}{c_i} \frac{1}{\sqrt{\pi}} \quad \exp -(w^2/c_i^2) + \left(\frac{w^2}{c_i^2} + \frac{1}{2} \right) \operatorname{erf} \left(\frac{w}{c_i}\right) \right\} \tag{41}$$

where

$$\operatorname{erf}(x) = \frac{1}{\sqrt{\pi}} \int_0^x e^{-t^2}\, dt \tag{42}$$

In the strongly subsonic case, $\frac{w}{c_i} << 1$ we get

$$F_D = -2\sqrt{\pi}\, n_i \cdot s^2 \cdot m_i \cdot c_i \cdot w \tag{43}$$

In the strongly supersonic case, $\frac{w}{c_i} >> 1$ we get

$$F_D = - \pi n_i \cdot s^2 m_i \cdot w^2 \tag{44}$$

b) <u>Distant Coulomb drag</u>

This is calculated using standard collision theory with minimum impact parameter = s and maximum impact parameter = λ_D the Debye length. In addition $m >> m_i$ and the plasma is again assumed to have Maxwellian velocity distribution. The solution is

$$F_C = 2\sqrt{\pi}\, n_i \cdot m_i \cdot \alpha^2 \; \frac{1}{c_i} \int_{-\infty}^{\infty} du \, \frac{u-w}{|u-w|^3} \quad \exp -(u^2/c_i^2)$$

$$\cdot \ln \frac{\alpha^2+\lambda_D^2(u-w)^4}{\alpha^2+s^2(u-w)^4} \tag{45}$$

where $\alpha = qe/m_i$.

Fig. 6 shows the relative strength of the direct particle drag and the distant Coulomb drag as a function of the velocity w in units of c_i the thermal speed for conditions corresponding to those in the inner plasmaspheres of Jupiter and Saturn. As can be seen, when the dust grain moves at subsonic speed with respect to the rest frame of the plasma, distant Coulomb collisions dominate by far, and the drag forces for both interactions are proportional to w. At supersonic speed the drag force due to direct collisions increases proportional to w^{+2}, whereas drag force due to distance Coulomb collisions decreases rapidly.

It has been shown by Morfill et al. (1980a) that in the strongly subsonic case if one assumes charge equilibrium, the Coulomb drag force can be approximated by

$$\left.\begin{aligned} F_C &\approx F_D \cdot I \\ \text{where} \quad I &= \int_0^{\infty} dx \, \frac{1}{x} \exp -x^2 \cdot \log \frac{1+\left(\frac{2\lambda_D}{s}\right)^2 x^4}{1+4x^4} \end{aligned}\right\} \tag{46}$$

with $x = (u-v)/c_i$. Setting $x_o = \sqrt{s/2\lambda_D}$ the integral is divided into two parts and approximated by

$$I \approx \int_0^{x_0} dx \frac{1}{x} x_0^{-4} x^4 + \int_{x_0}^{1} dx \frac{1}{x} \ln (1+(x/x_0)^4) \tag{47}$$

We get

$$I \approx \frac{1}{4} - \langle \ln (1+(x/x_0)^4 \rangle \ln x_0. \tag{48}$$

Putting $\langle \ln(1+(x/x_0)^4) \rangle \approx \frac{1}{2} \ln \frac{1}{x_0^4}$ we obtain for the typical values $s = 10^{-4}$cm and $\lambda_D = 10^3$ cm

$$I \approx 140 \tag{49}$$

in other words distant Coulomb collisions increase the drag force for subsonic grains, which are in charge equilibrium with the plasma, by a factor $\sim$140. This factor is insensitive to parameter changes since it only depends on them logarithmically.

III.6 Mutual collisions

Mutual collisions among dust particles can lead to grain destruction and fragment generation (high velocity collisions) or grain growth (low velocity collisions). By these effects dust particles are generated, destroyed or modified inside planetary magnetospheres. Low velocity collisions (relative speed $\lesssim$ 100 m/s) occur among particles in planetary rings, whereas particles having largely different orbits will collide at much higher speed. Interplanetary meteoroids will collide with particles in orbit about a planet with a typical speed of tens km/s. High velocity collisions produce a large number of fragment particles which couple differently to the magnetospheric environment than their parent particles. In addition high velocity collisions provide a source for neutral gas and plasma inside magnetospheres. Both effects will be briefly described.

a) High velocity collisions

From impact studies we obtain the following empirical relationships (see, e.g., Dohnanyi 1969; Gault and Wedeking 1969): When a small particle of mass m_p and velocity v collides with another body, we can get "erosive collisions" if the target is sufficiently large with respect to the projectile size, or we can get "catastrophic disruption" if the target is too small.

In erosive collisions the ejected mass is given by

$$m_e = \gamma m_p \tag{50}$$

where $\gamma \sim 5.10^{-10} v^2$ (v in cm/sec). The largest fragment ejected has a mass

$$m_L \sim 0.1\ \gamma m_p \tag{51}$$

and the size distribution of the ejected grains is

$$g(m) = C\ m^{-\beta} dm \tag{52}$$

where $\beta = 1.8$ and C is determined from

$$\gamma m_p = \int_0^{m_L} m\ g(m)\ dm \tag{53}$$

<u>Catastrophic disruption</u> occurs when the target mass is less than $\sim 100\ \gamma m_p$. Again the size distribution of the fragments follows a power law distribution (52) with $\beta \approx 1.8$ and C determined from

$$m_T = \int_0^{m_L} m\ g(m)\ dm \tag{54}$$

where m_T is the mass of the target particle. The mass of the largest fragment is, according to Fujiwara et al.(1977),

$$m_L = 1.66 \times 10\ E_p^{-1.24}\ m_T^{2.24} \tag{55}$$

where E_p is the kinetic energy in c.g.s units of the projectile with respect to the target particle.

Most fragment mass is ejected at a low speed (order of m/s) and only a very small fraction of the fragments ($\sim 10^{-5}$ of the total mass and only the smallest particles $m < m_p$) will be ejected at high speed (order of km/s) (cf. Gault and Heitowit 1963).

For recent applications of collision theory to ring systems see Morfill et al. (1980b), Burns et al. (1980) and Grün et al. (1980) for a discussion of the Jovian ring and Morfill et al. (1982b) for collision effects in the Saturnian ring system. Morfill et al. (1982b) estimate that the erosion time of Saturn's rings is only $\sim 5 \times 10^6$ years. However, for a large system like Saturn's rings, only a minute fraction of the ejecta is actually lost into the atmosphere or into interplanetary space. The rest is redistributed over the rings and forms a regolith of several cm depth on cores of larger ring particles (for a more detailed description of these effects, see Durisen, 1983). This picture is consistent with the hypothesis put forward by Smith et al. (1982) which says that the inner Saturnian satellites (inside about 6 R_S) have been disrupted by impacts and reaccreted several times since the formation of the Saturnian system.

High velocity impacts produce also vapor and ions (see,e.g., Gault et al. 1972, Fechtig et al. 1978, Hornung and Drapatz 1981). At impact speeds of, e.g., v = 30 km/s the vapor mass produced roughly equals the projectile mass (a factor of $\sim$ 3 higher

according to Gault et al. 1972, and perhaps even higher than that if one considers ice targets according to Lange and Ahrens, 1982). Morfill et al. (1982a) suggest that the neutral gas emitted by impact vaporization is responsible to a large part for the observed neutral atmosphere above Saturn's rings (Broadfoot et al., 1981). The residual ionization of the impact generated vapor cloud will be of the order of a few per cent (Hornung and Drapatz 1981) for mm-sized projectiles and the speed considered above. These highly time-variable impact plasma clouds interact with the planetary magnetic field after their density is sufficiently reduced by expansion. Morfill and Goertz (1982) propose that a collection of such clouds produced, e.g., by the impact of a swarm of interplanetary meteoroids onto Saturn's ring, may trigger the formation of spokes. Ip (1982) suggests that inside a distance of 1.625 R_S from Saturn these impact produced ions tend to move upward along the dipole field lines until they are lost into the ionosphere. Such a siphoning mechanism could lead to appreciable loss of ring material in this region. Northrop and Hill (1983), on the other hand, claim that the inner edge of the B ring has been caused by such a process (cf. section IV.1b).

During the crossing of Saturn's ring plane the Voyager 2 plasma wave instrument detected impulsive noise (Scarf et al., 1982) which has been interpreted as micron-sized par-

ticles hitting the spacecraft and producing charge pulses which were recorded by the instrument (Gurnett et al., 1983).

b) Low velocity collisions

We want to discuss the effects of low velocity collisions on the size distribution of E ring particles and estimate the time scale for particle growth. We will consider small perturbations of grain orbits by fluctuations in the plasma drag. Other rings or ring systems may be vastly different (e.g. Jupiter's ring, Morfill et al. 1980b, Burns et al. (1980), Grün et al. 1980, where destructive collisions are dominant).

The evolution of the size distribution f(s,t) in a spatially homogeneous system is given by

$$\frac{\partial f(s_1,t)}{\partial t} = -\int_0^\infty ds_2 f(s_1,t) f(s_2,t) \pi (s_1+s_2)^2 Q_{12} \langle (\Delta_{12}\delta v)^2 \rangle^{1/2}$$

$$+ \frac{1}{2}\int_0^{s_1} ds_3 f(s_2,t) f(s_3,t) \pi (s_2+s_3)^2 Q_{23} \left(\frac{s_1}{s_2}\right)^2 \langle (\Delta_{23}\delta v)^2 \rangle^{1/2} \tag{56}$$

The first integral is a loss term due to collisions of particle (1) with any other (which removes it from the size range s_1 to $s_1 + ds_1$) and the second integral is the growth of particles into the size range s_1 to $s_1 + ds_1$ by two body collisions bet-

ween particles (2) and (3). Q is a sticking probability (≤ 1) and $<(\Delta_{ij}\delta v)^2>^{1/2}$ is the r.m.s. value of the stochastic relative velocities between particles i and j. The case of interest for us corresponds to a weak perturbing force (the plasma drag on micron-sized dust particles in Saturn's E ring gives time scales for momentum exchange $\tau_f \approx 10$ years, see Morfill et al (1982b), in contrast to the correlation time of the perturbations τ_{K_o} which is short, i.e., the orbital period $\sim$ days). From Völk et al, (1980) we obtain for the case of stochastic gas drag forces $<(\Delta\delta v)^2>^{1/2} \approx 0.3$ km/s (for $\tau_f/\tau_{K_o} = 10^3$, nearly equal-sized grains and a stochastic plasma velocity component of 10 km/s). This is too small to cause fragmentation of most grains.

The collision rate between similar size grains is

$$\nu = 4\pi s^2 \, n < (\Delta\delta v)^2>^{1/2} \tag{57}$$

with $n = \tau/4\pi s^2 h$ the spatial grain density, τ the normal optical depth and the scale height h. Hence (57) becomes

$$\nu = (4\tau/h) < (\Delta\delta v)^2 >^{1/2} \tag{58}$$

i.e. the grain size cancels. For the E ring, we use the numbers of table 1 ($\tau = 10^{-6}$, $h = 10^{9}$ to 10^{10} cm). Then the collision time $\tau_{coll} = \nu^{-1} \sim 3000$ years. This is also the grain growth time (doubling the mass). Of course, the value for $<(\Delta\delta v)^2>^{1/2}$ is uncertain, but it is not a rapidly varying function of particle size or τ_f (cf. Völk et al. 1980). The comparison of the grain growth time scale by coagulation with loss time scales (eg. due to sputtering) will be discussed below (section on radial transport).

IV. Kinetic effects

IV.1 Gravito-electrodynamics

While the motion of the plasma (both thermal and energetic) within a planetary magnetosphere is almost totally controlled by electromagnetic forces, with planetary gravitation playing only a very secondary role (e.g., causing slow azimuthal drifts), the motion of the larger bodies such as satellites is overwhelmingly controlled by planetary gravitation, with gravitational perturbations by neighbouring satellites playing a secondary role. Even for cm and mm sized grains that populate the rings, the electromagnetic effects are negligible compared to gravity for any acceptable values of the surface potential (even for those values close to their field emission or electrostatic disruption limits). It is only when we consider grains of micron size (o.1μ - 5μ) that these two forces can become comparable for plausible values of the grain surface potential.

The gravitational force is given by

$$\vec{F}_G = - \frac{\mu m}{r^2} \hat{r} \tag{59}$$

where $\hat{r}$ is the radial unit vector and the Lorentz force is

$$\vec{F}_L = \frac{q}{c} (\vec{w} \times \vec{B}) \tag{60}$$

where q is given by (12) and c is the speed of light. With $|\vec{B}| = B_0 L^{-3}$ in the magnetic equatorial plane we obtain

$$\frac{F_L}{F_G} = k \frac{V_0 w_\perp}{s^2 L} \tag{61}$$

with the perpendicular (to the magnetic field) relative speed of the dust grain $w_\perp$ in cm/s, V_0 in volts, s in cm, L in planetary radii and the constant k. In the case of Jupiter it is

4×10^{-17} and in that of Saturn it is 5×10^{-18}. For a dust grain of size $s = 10^{-5}$ cm (0.1 μm) at a distance of L = 5 from Jupiter which moves at a speed $w_\perp = 5\times10^{6}$ cm/s and is charged to a surface potential of $V_o = 10$ V we get

$$F_L/F_G = 4. \tag{62a}$$

For the values $s = 10^{-4}$ cm, L = 2 , $V_o = 10$V and $w_\perp = 10^5$ cm/s we get in the Saturnian case

$$F_L/F_G = 2.5\times10^{-4} \tag{62b}$$

The values of F_L/F_G for negatively charged grains in prograde circular orbits, having different sizes and potentials at a distance of L = 5 from Saturn is shown in Fig. 7. Clearly, electromagnetic forces are most important for submicron-sized grains (0.1 μm $\leq s_\mu \leq$ 0.5 μm) in Saturn's E ring ($3.5 \leq L \leq 9$). Closer to the planet, in the region of the F ring and in the spoke region the dust particles have to be much smaller in order to be dominated by electromagnetic forces, because $w_\perp$ decreases and the surface potential V_o may be strongly reduced. At the co-rotation distance (L = 1.86), however, F_L/F_G = 0 even when the grain is charged.

Any attempt to bracket the range of F_L/F_G for the application of gravito-electrodynamics is necessarily arbitrary, but the range 10^{-2} to 10^{2} may be reasonable. It must be noted that even when $F_L/F_G \sim 10^{-2}$, the electric force on the grains is still many orders of magnitude larger than, for instance, the typical gravitational perturbing force of a nearby satellite. Therefore, while the grain orbit is largely controlled by gravitation, in this case the perturbations produced by electromagnetic forces are sufficient to give rise to various subtle effects that may be observable. We want now to study the general solution of gravito-electrodynamics and the stability of orbits.

a) General solution

The equation of motion of a charged dust grain in the planet-centered inertial frame is given by

$$\ddot{\vec{r}} = \frac{q}{m}\left(\vec{\mathcal{E}} + \frac{\dot{\vec{r}}}{c} \times \vec{B}\right) - \frac{\mu}{r^3}\vec{r} + \vec{F} \tag{63}$$

where $\vec{F}$ represents forces associated with the collisions with photons, plasma and other grains.

Within the rigidly co-rotating regions of the planetary magnetospheres, where the ring systems are observed,

$$\vec{\mathcal{E}} = -\frac{1}{c}(\vec{\Omega} \times \vec{r}) \times \vec{B} \tag{64}$$

where $\vec{\Omega}$ is the angular velocity of the planet. This is, of course, strictly applicable only when the Debye spheres of neighboring particles do not intersect, otherwise the electric fields of neighboring particles will also have to be included in $\vec{\mathcal{E}}$. The single-particle approach of gravito-electrodynamics needs some essential modifications in this case. However, a comparison of the co-rotational electric force (which is due to the radial polarization of the co-rotating plasme) with the electric force due to neighboring grains indicates that the former is orders of magnitude larger in this case, too. Consequently it is possible that the predictions of the single-particle gravito-electrodynamic theory is not seriously invalidated in this case, and may at least be correct to the first order. The main modification is a decrease in the grain potential in this case.

In the case of Saturn the magnetic moment and the spin vector are parallel (Connerney et al., 1982) within the observational uncertainties.

It is easy to show (Mendis et al., 1982a; Northrop and Hill, 1982a) that (63) and (64) admit circular orbits in the equatorial plane moving with angular velocity ω_G given by

$$\omega_G = \frac{\omega_{go}}{2} \left\{ -1 \pm \sqrt{1 + 4\left(\frac{\Omega}{\omega_{go}} + \frac{\omega_{Kep}^2}{\omega_{go}^2}\right)} \right\} \tag{65}$$

where ω_{Kep} is the local Kepler angular velocity and ω_{go} is the gyrofrequency

$$\omega_{go} = -\frac{qB}{mc} \tag{66}$$

Eq.(65) shows that two different motions are possible for a given grain. The plus sign in front of the square root corresponds to direct (or prograde) motion, while the negative sign corresponds to indirect (or retrograde) motion, for a negatively charged grain. For a positively charged grain, the minus sign in front of the square root gives a prograde motion while the plus sign gives a prograde or retrograde motion depending on the value of ω_{go}.

If a charged dust grain, moving in a circular orbit in the equatorial plane of the planet (whose magnetic moment and spin are strictly parallel), is subject to a small perturbation in the plane (e.g., by the gravitational tug of a nearby satellite), it has been shown (Mendis et al., 1982a, Morfill et al., 1982b) that the grain will perform a motion that can be described as an elliptical gyration about a guiding center which is moving uniformly in a circle with the angular velocity given by ω_G (Eq.(65)). The gyration frequency, ω, about the guiding center is given by

$$\omega^2 = \omega_{go}^2 + 4\omega_{go}\,\omega_G + \omega_G^2 \tag{67}$$

Also, if a and b are the semimajor and semiminor axes of this ellipse, it is shown that

$$\frac{b}{a} = -\frac{\omega}{2\omega_G + \omega_{go}} \tag{68}$$

with the minor axis aligned in the radial direction.

b) Stability of orbits

Not all the grain orbits are stable. Those which are must satisfy the condition $\omega^2 > 0$. One can use (65), (67), (68), together with this condition, to obtain the stable orbits at any given distance from the planet. The classes of stable and unstable orbits within the rigidly co-rotating portion of the Saturnian magnetosphere are exhibited in a general fashion in Fig. 8. Here $\alpha(=\omega_{Kep}/\Omega)$ is the independent variable and ω_G is the dependent variable. α varies from $\alpha = 2.5$ which corresponds to the Saturnian surface to $\alpha = 0.1$ which corresponds to $r = 10\ R_S$. Also the position of the synchronous orbit ($\alpha = 1$) and the F-ring ($\alpha = 0.7$) are indicated.

It is seen, for instance, that at the distance of the F-ring, negative particles of all sizes, from the smallest (co-rotating) particles to the largest (essentially Keplerian) particles moving in the prograde sense are stably trapped, as expected. Interestingly, there are several other distributions of particles too that can be stably trapped there. One of these is a set of retrograde negative particles, from the largest (Keplerian) particles to a moderatly large one moving with angular velocity $\cong -\Omega$. There are also

three distinct populations of positive prograde particles and another population of positive retrograde particles that can be stably trapped. One set consist of very small (positive) particles moving slightly faster than the co-rotation speed, while a second set consists of very large (positive) particles moving prograde slightly slower than the Kepler speed. These are clearly to be expected. Somewhat less obvious is the existence of two stable populations of large-to moderate-sized (positive) particles, one moving in the prograde sense, and the other moving in the retrograde sense. The populations of large-to moderate-sized (positive) prograde particles between curves B and C are unstable and are excluded.

Northrop and Hill (1982b) have also studied the stability of charged grains in the equatorial plane of Saturn to perturbations normal to the ring plane. For a grain of given specific charge there is a critical distance R_c such that grains with $r < R_c$ are unstable. Northrop and Hill (1982b) have argued that the prominent change in the ring brightness, which seems to start around 1.63 R_S, may be associated with the location of this stability radius at 1.625 R_S for grains of very large specific charge (q/m). R_C = 1.625 R_S corresponds strictly to "grains" with infinite specific charge and is therefore more appropriate for plasma. This effect is due to the fact that along a certain dipole field line the force acting on a charged particle may vary as a function of distance and latitude. This force can change from inward-pointing as gravity is the dominant force to outward-pointing with centrifugal force taking over. Fig. 9 shows these two regimes in the Saturnian magnetosphere. Ip (1982) has argued that the decrease of optical depth, by about a factor of 2 near 1.625 R_S is due to the field-aligned siphoning off of plasma formed inside this radius by the collision of interplanetary meteoroids with ring particles, whereas the collision-produced plasma outside this radius is confined to the equatorial plane and is not lost to the Saturnian ionosphere.

Northrop and Hill (1983) pointed out that the stability limit at 1.625 R_S corresponds to highly charged particles which move in circular orbits i.e. with the local co-rotation speed. However, if highly charged ($|q/m| \gtrsim 7.5$ Coul/g) particles are launched in the ring plane at the local Kepler velocity then their stability limit is found almost exactly at the inner edge of the B ring (Northrop and Hill, 1983). Clusters of water molecules possibly created by micrometeoroid impacts onto the ring would satisfy this condition, according to these authors.

From Fig. 8 it is clear tnat negatively charged, prograde grains outside the synchronous orbit move with an angular velocity ω_G which is larger than the Kepler angular velocity at that distance. Since ω_G depends on ω_{go} and therefore on the grain size s, for a given potential there would be grains of a certain size which would move with the same angular speed Ω_{Sat} as a satellite interior to the grain orbit. This means there is an exact 1:1 orbit-orbit resonance with such a satellite. Large positively charged grains outside the synchronous orbit move with ω_G which is smaller than ω_{Kep}. These particles could have a 1:1 resonance with a satellite outside the grain orbit. A similar situtation clearly does not arise in the purely gravitational case. This magneto-gravitational resonance would, for instance, arise between a certain size grain in the F-ring and its nearby satellites S27 and S26, depending on the charge state of the grains.

It must be stressed here that, unlike a pure gravitational resonance, which affects particles of all sizes equally, the magneto-gravitational resonance picks out a particular grain size s_c for a given potential V_0. Of course, grains with sizes close to s_c (on either side of it) will be strongly affected because their angular velocities will be close to that of the perturbing satellite, and will therefore remain in the vicinity of that satellite for long periods of time. If we consider such a particle with a

gyration frequency ω about a guiding center moving with angular velocity ω_G, it can be shown (Mendis et al., 1982a) that the grain will move in an undulating orbit having a wavelength λ given by

$$\lambda \doteq \frac{2\pi r}{\omega} (\omega_G - \Omega_{Sat}) \tag{69}$$

where Ω_{Sat} is the angular velocity of the perturbing satellite. Furthermore, as each successive grain of the same size in the ring moves over the satellite it will be subject to the same perturbation and will therefore follow the same path as its predecessor in the frame of the satellite. Consequently, all the grains will move in phase to form a wavy pattern with the wavelength λ in the frame of the perturbing satellite. It has been proposed by Mendis et al., (1982a) and Hill and Mendis, (1982b) that the waves observed in the F-ring are formed this way. However, they require that the dust particles are charged to $V_0 = -38V$. As mentioned earlier, collective self-shielding of the closely spaced dust population may rule out such large potentials.

Hill and Mendis (1982b) have also shown the existence of another type of resonance, which they call "gyro-orbital resonances" for charged dust grains. This is due to the modulation of the grain potential with the orbital period as the grain moves in and out of the planet's shadow. Consequently, if the gyro-period of the grain is in resonance with the grain orbital period, the grain is strongly affected by this effect and its orbital eccentricity grows until it is removed by collisions with neighbouring grains. Hill and Mendis (1982b) propose this effect to be responsible for clearing small isolated gaps in Saturn's B ring from highly charged sub-micron-sized dust particles.

IV.2 Radial transport

Radial transport of dust particles can be described in two extreme ways: 1) large particles, basically on Keplerian orbits, which are gradually transported either systematically or stochastically and 2) small particles, which are electromagnetically dominated and are transported systematically or stochastically.

The method that we use to describe this transport employs a "diffusion-convection" formalism. In terms of the integrals of motion I_i and their associated cyclic variables α_i, this yields for the evolution of the distribution function, f, in space and time

$$\frac{\partial f}{\partial t} + \frac{\partial}{\partial I_i}\left(\frac{dI_i}{dt} f - \frac{1}{2} < \frac{\Delta I_i \Delta I_j}{\Delta t} > \frac{\partial f}{\partial I_j}\right) = 0 \qquad (71)$$

where $\frac{dI_i}{dt}$ is a systematic change in I_i caused by a systematic interaction (e.g., momentum exchange with an ambient medium, i.e. particle friction, plasma drag). The transport coefficient in angled brackets requires knowledge of the power spectrum of perturbing forces. We are dealing with "resonant" phenomena, i.e. only those frequencies in the perturbations are picked out which are multiples of the particle's natural frequencies (e.g., orbital frequency, gyrofrequency).

From Morfill et al. (1982b) we obtain, e.g., a systematic radial drift velocity due to friction:

$$v_r \approx -\frac{2a_s}{\tau_f}\left(1 - \frac{\Omega}{\omega_{Kep}}\right) \tag{72}$$

where a_s is the semimajor axis, Ω the planetary rotation rate and ω_{Kep} is the local Keplerian angular velocity. The frictional coupling time scale is τ_f. In the case of "large" particles, we have the constants of motion I_i and the associated cyclic variables given in table 3 (Barge et al. 1982, Hassan and Wallis 1982). One of the four integrals of motion is redundant.

a) <u>The adiabatic motion of charged dust grains</u>

In the case of "small" particles, which are electromagnetically dominated, the integrals of motion and associated cyclic variables are given in Table 4 (see eg. Schulz 1975, Morfill 1978). The frequencies are the gyrofrequency (associated with I_1), bounce frequency (I_2) and longitudinal drift frequency (I_3).

Northrop and Hill (1982a) extended the usual adiabatic theory of charged particle motion (see Northrop, 1963) to include the complication of a variable grain charge q(t). The charge on a grain is modulated by variations of the relative speed between the grain and the plasma and by gradients in the plasma density and energy. Since the time scale for charging and discharging is finite, it introduces a phase lag in the charge with respect to the orbital position of the grain. The adiabatic theory developed is quite general and is applicable to the case when the magnetic moment and the spin vector of the planet are at any arbitrary angle. Converting the equation of motion to the frame rotating with the planet, Northrop and Hill (1982a) showed that the charged grain may be regarded as moving in an "pseudo-magnetic field" $\vec{\mathcal{B}}$ given by

Table 3: Transport of gravitationally dominated dust grains

Integral of motion	Cyclic variable
$I_1 = -ma_s^2\omega_{Kep}/2$	$\alpha_1 = -\omega_{Kep}T$
$I_2 = m\omega_{Kep}a_s^2(1-e^2)^{1/2}$	$\alpha_2 = -\omega_p$
$I_3 = I_2 \cos(i)$	$\alpha_3 = -\Omega$
$I_4 = -ma_s^2\omega_{Kep}^2/2$	$\alpha_4 = T$

$\omega_{Kep}^2 = GM/r_o^3$, where r_o is the initial particle position from the planet center e = eccentricity, i = inclination, T = time of pericenter passage, ω_p = elongation of pericenter and Ω = longitude of ascending node. The integrals of motion are: I_1: action, I_2: total angular momentum, I_3: -component of angular momentum, I_4: total energy.

Table 4: Transport of electromagnetically dominated grains

Integral of motion	Cyclic variable
$I_1 = p_\perp^2/2mB$	$\alpha_i \equiv \frac{\partial W}{\partial I_i}$
$I_2 = \oint p_{\parallel}\, ds$	
$I_3 = \frac{q}{c}\,\phi$	

$p_\perp$ is the component of particle momentum perpendicular to the magnetic field $\vec{B}$, $p_{\parallel}$ is the parallel component, the integral $\oint ds$ extends along the field line to the mirror points, ϕ is the magnetic flux enclosed by the drift shell. W is the total (kinetic + potential) energy of the particle. The integrals of motion are the three adiabatic invariants.

$$\vec{\mathcal{B}} = \vec{B} + 2mc\vec{\Omega}/\langle q(t)\rangle \tag{70}$$

where $\langle q(t)\rangle$ is the value of q(t) averaged over a gyrocycle and an equivalent electric field $\frac{m}{q(t)} \nabla(\frac{1}{2} r^2\Omega^2 - \phi_g)$, where ϕ_g is the gravitational potential and r is the axial distance.

The charge q(t) varies systematically with its gyrophase about the guiding center. Consequently the circle in which the grain gyrates rocks at the gyrofrequency. Since the variation of q(t) is rather small, the angle through which the circle rocks is also small. The average plane of this circle is perpendicular to the "pseudo-magnetic field" $\vec{\mathcal{B}}$.

From this it is apparent, as expected, that electrons and ions with very small m/q_o gyrate very nearly in a plane normal to $\vec{B}$, whereas bodies having large m/q_o gyrate in a plane very nearly normal to $\vec{\Omega}$.

In the intermediate particle size range, only direct orbit trajectory integrals can be used for a correct transport description. In conjunction with stochastic forces, this is very tedious and time consuming, but there seems to be no alternative (Hill and Mendis 1980). The two situations involving

tedious and time consuming, but there seems to be no way around this (Hill and Mendis 1980). The two situations involving electromagnetic perturbations, which are amenable to analytical Fokker-Planck type analysis are: 1) Io-produced "smoke" particles, which may escape into the magnetosphere of Jupiter (Johnson et al. 1980, Morfill et al. 1980a, b, c, d), and are probably magnetically-dominated, and 2) Saturn's E ring (Morfill et al.1982b) which is probably gravitationally-dominated.

b) Systematic drift

Two classes of processes have been considered so far: friction with the ambient plasma and radiation pressure drag on the one hand (Morfill et al.1980a, Morfill et al.1982b), and systematic charge variations caused by the dust grain motion and/or plasma density gradients on the other hand (Northrop and Hill 1982a).

In the case of magnetically dominated particles, one would expect systematic charge variations to occur at the particle's gyrofrequency. These charge variations can be caused by the dust grain's own velocity variation with respect to the ambient plasma, or by a radial plasma gradient or a radial gradient in the electron energy.

As shown by Northrop and Hill (1982a), a radial drift motion, always directed to the synchronous radius, is set up in the former case. The effect is relatively subtle, as the authors point out, since it may only amount to a charge variation $\delta q/q \cong 10^{-3} - 10^{-4}$ (i.e. of the order of 1 electron charge or even less) per gyroperiod In the Io plasma torus, where the plasma density is higher, the effect will be correspondingly more important.

A plasma gradient may lead to a more significant radial drift effect. The particle gyroradius is inversely proportional to the magnetic field strength (for constant particle velocity), or,

$$r_g \cdot R_g L^3 \tag{73}$$

where R_g is the gyroradius the particle would have at the planetary surface. The plasma density, in general, is described by

$$n \cong N_o L^m \tag{74}$$

where N_o is the extrapolated value to the planet's surface. The plasma density fluctuation sampled by the dust grain during one gyroperiod is

$$\frac{\delta n}{n} = m \frac{2r_g}{R\,L} \tag{75}$$

where R is the planetary radius. Substituting (73) and writing $R_g = \varepsilon R$ with $\varepsilon << 1$, gives

$$\frac{\delta n}{n} = 2\ m\ \varepsilon\ L^2 \tag{76}$$

For typical values (e.g., in Jupiter's inner magnetosphere) $m = -2$, $\varepsilon = 10^{-2}$ (corresponding to $\sim 0.1\ \mu m$ dust grains) we get

$$\frac{\delta n}{n} = 0.04\ L^2 \tag{77}$$

i.e., a few percent. The potential V of the dust particle is determined by the balance between plasma electron flux and photoelectron flux K (electrons/cm^2 sec), at least in sunlight (cf. equations (6) and (9))

$$\pi s^2 n\ \ c_e\ \ \exp\ (eV_O\ /\ E_e) = \pi s^2\ K \tag{78}$$

Differentiating (78) yields

$$\frac{edV_O}{E_e} = \frac{dn}{n} \tag{79}$$

which shows that the surface potential fluctuates with the plasma density. The associated charge fluctuation over a gyroperiod is then $\delta q/q \approx \delta n/n$, i.e., it is significantly larger than the charge fluctuation induced by the dust motion itself.

As pointed out by Northrop and Hill (1982a), periodic charge fluctuations destroy the invariance of the grain's magnetic moment and induce a radial motion. The direction of the drift depends on the sign of the plasma density gradient. Friction with the ambient plasma, and radiation pressure drag leads to a decay of the particle's gyroradius, as pointed out by Morfill et al. (1980a). This also leads to a decrease in

the radial drift induced by electromagnetic forces, both systematic and stochastic ones.

In the case of gravitationally dominated particles, the drag forces have two effects. They circularize the orbits (plasma) and in the case of radiation pressure they induce large amplitude oscillations due to the daylight - shadow variations (Peale, 1966, Burns et al., 1979, Mignard, 1982). At the same time the orbital energy of the particles is changed (increased by the plasma drag outside the synchronous orbit, decreased by the radiation pressure drag). As an example, we demonstrate this with Saturn's E ring.

In the inner magnetospheres the plasma drag dominates over radiation pressure considerably. The associated systematic radial drift velocity is, using Saturn's plasma environment (Morfill et al.1982b):

$$v_r(4<L<7.5) \approx v_{ro} \frac{r}{\rho s} \tag{80a}$$

$$v_r(7.5<L<9) \approx v^*_{ro} \frac{r}{\rho s} \tag{80b}$$

where ρ is the particle's density (we take $\rho = 1$ g/cm^3 and v_{ro} is a constant $\approx 4\times10^{-13}$ and $v^*_{ro} \approx 4\times10^{-15}$. Distant Coulomb collisions have been taken into account. If we assume that the particle's inclinations are not strongly affected by the drag forces, we have to solve (in the absence of stochastic forces):

$$\mathrm{div}\ (v_r n)\cdot + n/\tau_S = 0 \tag{71}$$

for the simplest scenario, where n is the dust particle spatial

density, and τ_S is the loss rate due to sputtering. Sputtering losses introduce a term $\frac{\partial}{\partial m}(\frac{dm}{dt})n$, which we have simplified into a particle loss term, on account of the fact that below a certain size the dust particles are essentially invisible.

The solution to (81) for a general $v_r(r)$, $\tau_s(r)$ is

$$n = n_o(\frac{r_o}{r})^2 \frac{v_r(r_o)}{v_r(r)} \exp(-\int_{r_o}^{r} \frac{dr}{\tau_S v_r}) \tag{82}$$

where the particle source is at $r = r_o$. From (80) this becomes

$$n \approx n_o (\frac{r_o}{r})^3 \exp(-\int_{r_o}^{r} \frac{dr}{\tau_S v_r}) \tag{83}$$

The boundary condition at r_o is

$$S = v_r n \,|_{r \to r_o} \tag{84}$$

where S (particles/cm^2 sec) is the source strength and is presumed to be known. Then

$$n \approx \frac{S\rho s}{v_{ro} r_o} (\frac{r_o}{r})^3 \exp(-\int_{r_o}^{r} \frac{dr\ s\rho}{\tau_S v_{ro} r}) \tag{85}$$

From Table 2 we find

$$\left.\begin{aligned} \tau_S(4 \le L \le 5) &= 1.8 \times 10^{11} \text{ sec} \\ \tau_S(5 \le L \le 7.5) &= 4.5 \times 10^{9} \text{ sec} \\ \tau_S(L > 7.5) &= 6 \times 10^{10} \text{ sec} \end{aligned}\right\} \tag{86}$$

Then we get $n = \frac{S\rho s}{v_{ro} r_o} \left(\frac{r_o}{r}\right)^{3+s\rho/\tau_S v_{ro}}$, and changing to $L \equiv r/R_S$ as a convenient notation, we obtain for micron size grains:

$$\left.\begin{aligned} n(4 \le L \le 5) &\approx 0.01S \left(\frac{4}{L}\right)^{3+1/720} \\ n(5 \le L \le 7.5) &\approx n(L=5) \left(\frac{5}{L}\right)^{3+1/18} \\ n(L > 7.5) &\approx n(L=7.5) \left(\frac{7.5}{L}\right)^{3+5/12} \end{aligned}\right\} \qquad (87)$$

This is a rather flat distribution not compatible with the E-ring observations although it is clear that the density drops off faster beyond L = 7.5. Diffusion due to fluctuating drag forces (e.g., caused by changes in the plasma density) will smear this distribution out even further. However, absorption by the moons Tethys, Dione and Rhea may play a role too, reducing the dust particle density as the grains are convected past, out of the Saturnian system. Absorption depends on the typical time scale, t_e, between distant encounters between the moon (orbiting at radius y = 1) and the ring particles (orbiting at radius $1 \pm \Delta y$). For $\Delta y \ll 1$, we get

$$t_e \cong \frac{8\pi R_S^{3/2} L^{3/2}}{\sqrt{\mu_S}\,\Delta y} \qquad (88)$$

where $R_S L$ is the radial distance of the moon from the planet center. This must be compared with the convection time across $2\Delta y$:

$$t_c \cong 2R_S L\,\Delta y/v_r \qquad (89)$$

$R_S L \cdot \Delta y$ is a few satellite radii, denoting the "sphere of influence" of the particular moon.

The absorption by the moon is then given roughly by

$$\eta \cong \frac{n(1+\Delta y)}{n(1-\Delta y)} \approx e^{-t_c/t_e} \tag{90}$$

The ratio t_c/t_e in the region $4 < L < 7.5$ is

$$\frac{t_c}{t_e} = 2.27\text{x}10^{-6}\ R_{Sat}^2\ s_\mu\ m^2\ L^{-7/2} \tag{91}$$

where m is the number of satellite radii (R_{Sat} in km) defining the sphere of influence ($m \sim 5$). In the region $L > 7.5$ t_c/t_e is a factor 100 smaller. For Tethys this yields $\eta \approx 0.95$, for Dione we obtain $\eta \approx 0.97$ and for Rhea $\eta \approx 0.18$.

Combining the results of this analysis (see also Morfill et al.1982b) we obtain the following qualitative picture (bearing in mind that there are large uncertainties in the sputter rates and in the somewhat arbitrary choice for satellite absorption):

1) dust grains are created somehow on the moon Enceladus at $L \cong 4$

2) they are transported outwards mainly by plasma drag.

3) sputtering and geometrical effects lead to a slowly decreasing grain density ($\sim L^{-3}$) as well as normal optical depth ($\sim L^{-2}$).

4) absorption by Saturn's moons leads to further grain reduction. This is particularly important for Rhea, because at $L = 8.7$ the radial drift due to plasma drag is small.

In principle the optical and trapped particle absorption signatures can be understood by invoking these processes.

c) Stochastic transport

Two processes leading to stochastic particle transport have been described in the literature. For magnetically-dominated particles, gyrocenter diffusion caused by stochastic charge variations is important (Morfill et al.1980a,d), For gravitationally-dominated particles stochastic forces lead to a diffusion of the particle orbits, in particular the orbital energy (Morfill and Grün 1979a,b, Consolmagno 1980), Barge et al.1982, Hassan and Wallis 1982, Morfill et al.1982b). Specific processes are magnetic fluctuations, and plasma drag.

Fig.10 shows the calculated dust particle diffusion coefficient for magnetically dominated particles in the Jovian magnetosphere (Morfill et al. 1980a) caused by random charge fluctuations. The plasma model used is indicated in the figure (L dependence of density n_i and electron energy E_e). The Io torus was not specially considered here. The quantity v^2s^4, (v = particle velocity = injection velocity into the corotating frame, s = particle radius) was kept as a parameter.

Fig. 11 shows the spatial dependence of Io injected "smoke" particles, with $v^2s^4 \equiv 10^{-9}$, inside the Io radius (Morfill et al.1980d). Losses by sputtering were shown to be relative minor, and plasma drag was not considered (the plasma drag would be partially cancelled by the plasma gradient induced drift mentioned earlier, so that the net effect would be a slightly faster decrease of the particle density towards the planet than the value shown in the figure).

We will not repeat the derivation of the spatial diffusion coefficient here (see Morfill et al.1980a). The physical reason for the diffusion is the following (c.f. Fig. 12): During a gyration about a field line, a dust particle (carrying a surface charge of, e.g., 1000 electrons) undergoes normal statistical charge fluctuations on a time scale comparable to the gyro period (e.g. $\pm \sqrt{1000}$, in the time Δt, which the particle needs to come into charge equilibrium). As a result, the gyroradius fluctuates statistically, the particle loses knowledge of "its" field line and the result is a "gyrocentre diffusion" across the magnetic field.

For gravitationally-dominated particles, short period stochastic charge fluctuations are only of minor importance, since by definition electromagnetic forces are much smaller than gravity. (This is even more so the case for perturbing electromagnetic forces, in particular when we consider that resonances at the particle orbital period, or a multiple thereof - but then with much reduced scatter efficiency -, are required to evoke energy changes and real orbit diffusion). Long period fluctuations in particle charge (and hence fluctuating electromagnetic forces) on the time scale of an orbital period may occur via long period plasma variations. These plasma variations may be caused by solar wind interaction with the magnetosphere, growth and decay of ring currents, nightside plasmasheet changes, flux tube interchange instabilities etc. Superimposed on the normal stochastic charge fluctuations is then another, also stochastic, long period charge fluctuation. Relevant frequencies are those of the external (solar wind) fluctuation

(periodicity ∿ 100 hours, if we consider corotating interaction regions, solar flares, sector boundaries, etc.), the plasma azimuthal drift period, the corotation period (∿ 10 hours) and the dynamical changes in the magnetosphere (ring currents, substorms, etc.) which could be again of the order 100 hours (unfortunately very little is known about this for Saturn's magnetosphere, and extrapolation from the Earth's magnetosphere is certainly not straightforward!). However, this discussion shows that one may certainly expect plasma parameter variations over the relevant time scales (days); their strength, however, is a subject for speculation at this stage.

Morfill et al. (1982b) have calculated the diffusion coefficient associated with such charge fluctuations. The result is

$$\kappa \approx \frac{\langle \Delta\omega_g^2 \rangle (\Omega - \omega_{Kep})^2 \langle \Delta t \rangle^4}{4(\tau_p + \langle \Delta t \rangle)} \tag{92}$$

where $\langle \Delta t \rangle$ is the mean duration of a different plasma "state" (e.g., higher/lower density), τ_p is the mean period between such "states", and $\Delta\omega_g$ is the induced fluctuation in the dust particle gyrofrequency,

$$\Delta\omega_g = B\Delta q/mc \tag{93}$$

The diffusion time scale

$$\tau_{diff} = r^2/\kappa \tag{94}$$

is then evaluated

$$\tau_{diff} \cong 6\times10^3 \frac{s_\mu^4 \, L^6}{\langle\varepsilon_i^2\rangle V_o^2} \quad \text{years} \tag{95}$$

where V_o is the grain potential in volts, s_μ is the grain radius in microns, and $\langle\varepsilon_i^2\rangle^{1/2} \equiv \delta q/q$. As an example, in the E-ring at L = 6, with $\langle\varepsilon_i^2\rangle^{1/2} \equiv 0.1$ and $V_o = 100$ volts mean surface charge, we obtain $\tau_{diff} \cong 3\times10^6$ years. This is considerably larger than the convection time or the sputter loss time, so that a pure convection-loss description as the one employed earlier seems justified, in spite of the large uncertainties in numerical values.

V. Observations

The main emphasis of this review paper has been the detailed discussion of the individual effects comprised in dust magnetosphere interactions. Occasional references to observations are given in the previous paragraphs. In the following we want to summarize observations in the Earth's, Jupiter's and Saturn's magnetospheres which are related to dust-magnetosphere interactions. We should caution that electromagnetic phenomena have been indicted in most of these observations because they could not easily be interpreted otherwise. Direct observations, e.g., of charged dust grains are scarce. In interplanetary space the dust experiment on board the Helios spaceprobe detected only 4 dust particles carrying a significant charge out of more than 200 observed particles (Grün et al., 1983). Also, as will be discussed below, direct observations of charged dust grains on the moon have been made (Berg et al., 1976). The next opportunity to observe directly charged dust particles will be by the dust experiments on board of the Galileo and ISPM space probes

which will perform in situ measurements of dust particles and their charges in interplanetary space and in the Jovian magnetosphere.

Direct measurements of complete orbits of charged dust particles in planetary magnetospheres are not possible: therefore their dynamics has to be infered from observations of an ensemble of dust grains. Remote sensing of dust particles by scattered or absorbed light or by high energy particle absorption yields important but limited information on the integral cross-sectional area or the mass density of dust particles. Only the combination of remote observations of the large scale distribution with in situ measurements of the dynamical state (mass, velocity and charge) of individual particles can support theoretical predictions. Therefore some of the observations reported below have been only tentatively related to dust-magnetosphere interactions.

V.1 Dust in the Earth's magnetosphere

In situ observations of dust particles near the Earth by the HEOS 2 micrometeoroid experiment (Hoffmann et al. 1975a,b) showed that the impact rate onto the sensor varied strongly within the Earth's magnetosphere inside 10 Earths radii (auroral zones). These short-term enhancements of the particle flux have been interpreted by Fechtig et al (1979) as fragmentation products of fragile large meteoroids in the 10 to 10^6 g mass range. These bodies receive a large negative surface charge (corresponding to a surface potential of several 100 V) when they travel through the auroral zone at about 10 Earth radii. This leads to electrostatic fragmentation (refer above) if the mechanical structure of the parent meteoroids is loose enough, and a "swarm" of small particles is produced. From the

observed particle swarms the authors were able to estimate the mass of the parent meteoroids and from the viewing directions of the sensor they could correlate them with type III fireballs (Ceplecha and McCrosky 1976). The masses and the fluxes of the parent meteoroids are in agreement with the corresponding fireball values.

Electrostatic transport of lunar surface dust was first suggested by Gold (1955) on the basis of theoretical considerations. Observationsl evidence came from optical observations of horizon glow by the Surveyor spacecrafts that revealed that dust is elevated several tens of centimeters above the lunar surface (Rennilson and Criswell, 1974). The authors conclude that surface particles are charged up and levitate due to intense electrostatic fields ($\sim$ 500 V cm^{-1}). They believe electrostatic transport is the dominant local transport mechanism of lunar fines. In situ observation of levitated dust on the lunar surface has been reported by Berg et al. (1976). The Lunar Ejecta and Meteorites (LEAM) experiment, placed on the moon by the Apollo 17 astronauts recorded a strongly enhanced flux of charged dust particles around times when the terminator passes over Apollo 17 site (see Fig. 13 from Berg et al., 1976). The three sensors (facing up, to the east and to the west) detected different impact rates during the terminator crossing and these indicate a flux of charged particles directed across the terminator. A detailed model of the lunar dust transport which takes into account these observations has not yet been developed.

Dust has been observed not only in the immediate vicinity of the lunar surface but Severny et al. (1974) reported that

the photometer on board the Lunokhod 2 vehicle measured scattered light extending up to the height of at least 260 meters above the surface. Visual observations of streamers and local horizon illuminations by the Apollo 8, 10, 15 and 17 astronauts before Apollo sunrise give evidence of high concentrations of dust up to the altitude of the spacecraft (120 km; cf. McCoy and Criswell,1974). Again the physical implications of these observations are not fully understood.

V.2 The Jovian ring

Voyager observations of the Jovian ring system have been described by Owen et al. (1979), Jewitt (1982), Jewitt and Danielson (1981) and reviewed by Burns et al. (1980,1982). The Jovian ring system consists of three components: the bright ring, the faint disk and the even more tenuous halo. Many particles in the bright ring are micron-sized (Jewitt and Danielson, 1981, Grün et al. 1980). At a surface potential of 10 V (Morfill et al. 1980b) these particles are gravitationally dominated and only plasma drag, sputter erosion and mutual collisions are important for their dynamical evolution. The particles in the faint disk, since they are highly concentrated towards the Jovian equatorial plane, must have their motions dominated by gravitational forces. Therefore they cannot be much smaller than those in the outer bright ring. They are probably derived from this outer ring and drawn inward by plasma drag and radiation pressure drag (Morfill et al. 1980b, Burns et al. 1980).

A tenuous ring envelops the other ring components with a characteristic dimension of 10^4 km, normal to the plane of the bright ring. This out-of-plane material forms a broad lenslike halo, the outer limit being beyond 1.8 R_J and having a slight north/south asymmetry with respect to the bright ring (Jewitt and Danielson 1981). This vertical extent can easily be explained by assuming its particles to be quite small ($s \approx 0.1\ \mu$ m) (Morfill et al. 1980b, Consolmagno, 1980, Grün et al. 1980). The motion of these particles is strongly influenced by electromagnetic effects and the tilted Jovian magnetic field results in an out-of-plane force. We may regard these particles as being injected locally by collisional fragmentation and erosion of ring and disk particles and mirroring in the "pseudo-magnetic field" $\vec{\mathcal{B}}$ given in equation (70). The average plane of their orbit is perpendicular to $\vec{\mathcal{B}}$, the axis of which lies between the Jovian magnetic dipole axis $\vec{B}$ and the rotation axis $\vec{\Omega}$. Burns et al. (1980) pointed out that the halo seems not to be symmetric about the magnetic equator but rather about the rotational equator. Also the lenslike shape of the halo which has its thinnest dimension near the bright ring while it is thickest near the planet is puzzling. To solve these questions detailed studies of the evolution of ring, disk and halo particles have to be carried out and improved photometric models have to be developed which take spacially varying particle sizes into account.

Johnson et al. (1979) showed that the volcanic activity which was discussed on the Jovian satellite Io does not only

lead to the ejection of copious amounts to gas into the Jovian magnetosphere, but can also be regarded as a source of small dust grains. It was suggested by Johnson et al.(1980) that these "smoke" particles are able to leave the satellite if their radii are smaller than $\sim$ 0.1 μm. These particles become electrically charged by the ambient plasma and are removed from the gravitational field of Io through the influence of the Jovian magnetic field which sweeps past Io at a speed of $\approx$ 50 km/s. Morfill et al.(1980a) showed that for such small particles, and a typical particle surface potential of $\sim$ 10 volts, the subsequent motion in the magnetosphere is dominated by electromagnetic forces. The particle motion is practically adiabatic, i.e., the particles gyrate about their field line, corotate and execute bounce motions between their mirror points. Their main transport process in the magnetosphere is diffusive, the stochastic element in the particle motion is due to random charge fluctuations. It has been proposed by Morfill et al.(1980b) and Grün et al.(1980) that these sub-micron-sized particles produce the visible ring particles by collisions with km-sized parent bodies ("mooms", Burns et al.1980). However, these sub-micron-sized Io particles have not yet been directly observed and their existence has to be proven by the forthcoming Galileo mission.

V.3 Saturn's ring system

Micron- and sub-micron-sized grains have been identified in the dense A and B rings especially in the spokes region and they dominate the populations in the outer F, G and E ring.

Dust-magnetosphere interactions may play an important role in determining the structure of Saturn's E, G and F ring. Plasma drag, sputtering, as well as diffusion of orbits due to plasma induced charge fluctuations appear to be important for dust particles with radii less than ∿ 10 μm (cf. Morfill et al. 1982b). For the E ring these processes may have caused the broad extent of the dust distribution within Saturn's magnetosphere (cf. paragraphs on sputtering and radial transport for a more specific discussion). Any calculation of a detailed E ring profile must take space variable loss of particles into account as well as transport and diffusion processes. Because of the short lifetimes of dust particles in that region due to sputtering and particle transport, an active source for E-ring particles is required, which is probably Enceladus.

During the crossing of the ring plane at a distance of 2.88 R_S which is just at the edge of the G ring the plasma wave experiment of Voyager 2 detected intensive impulsive noise (Scarf et al, 1981). This noise has been attributed to small micron-sized particles hitting the spacecraft which produce charge pulses by impact ionization. Gurnett et al. (1983) were able to derive the masses of the dust grains from the observed signals. The results obtained show that the mass distribution varies as m^{-3}, and that most of the particles detected had radii in the range from 0.3 to 3 μm. The observation of micron-sized particles in the G ring which are subject to dispersive forces, like the E ring particles are, and a ring which is nevertheless quite narrow, implies that it is either a recent phenomenon (∿10^3 years) or it must be confined in some way, presumably by

shepherding satellites: accordingly it should perhaps have a structure resembling that of the F ring.

The complicated, time variable, narrow structure (braids, kinks, multiple strands) of the F ring is heavily influenced by the gravitational interaction of the shepherding satellites 1980S26 and 1980S27. It has been proposed by Morfill et al.(1982b) that coherent ring displacements caused by plasma sheet induced charge variations on the grains are observable in the F ring in the form of waves which may subsequently evolve into kinks. Mendis et al,(1982a) and Hill and Mendis (1982b) suggest that the wave pattern observed in the F ring originates from a magnetic-gravitational resonance between charged dust grains of a specific size and a shepherding satellite. Whether these effects will work depends on the plasma conditions at the F ring and the charge state F ring particles may acquire. Purely gravitational interaction has been considered by Showalter and Burns (1982) in order to explain the hinks and clumps observed by Voyager. However, the observed braiding is not understood at all.

During both Voyager encounters with Saturn, the Planetary Radio Astronomy experiment detected strong discrete episodic bursts of radio emission, termed Saturn electrostatic discharges (SED, Warwick et al., 1981, 1982). Although Evans et al. (1982) claim that the source for the SED is located in Saturn's B ring no physical process has been forwarded to explain the generation of SED in the ring. Recently Kaiser et al. (1983) show that SED are consistent with an extended lightning storm system in Saturn's atmosphere.

Micron-sized particles cause the almost radial spokes in the B ring. Smith et al.(1981) noted that spokes appear dark in back-scattered light but appear bright against the background B ring in forward-scattered illumination, suggesting micron-sized particles elevated above the ring plane to be responsible for this phenomena. A theory of spokes has to explain this and the following observed spoke characteristics (Smith et al,1981, 1982, Porco and Danielson 1982, Grün et al. 1982): Spokes have been observed in the B ring between about 100,000 km to 117,500 km from Saturn's center. They commonly appear wedge-shaped, with a vertex at a distance of 112,500 km (co-rotation distance). Their width at the base (towards Saturn) varies from about 2,000 km to 20,000 km and their radial extension is about 3,000 km to 12,000 km. However, narrow (typically 500 km in width) filementary spokes have been observed outside a radial distance of 110,000 km mostly joined with a wider spoke further in.

Several narrow spokes were observed during formation along radial lines in the sunlit portion of the ring. The formation time is typically $\lesssim$ 5 min for a 6,000 km long spoke. The rate of spoke formation is highest at the morning ansa outside Saturn's shadow. Spokes are nearly radial or tilt away from radial in such a way that Keplerian motion will continue to tilt them further. From measurements of the angular velocity of spoke edges it was shown that in most cases both spoke edges revolve with Keplerian speed. However, a few spokes have been found where only one edge revolves with Keplerian speed whereas the other edge stays radial and co-rotates with

Saturn. Due to this their width increases with time. Spoke activity varies within the measurement errors of ± 22 min with a period of Saturn's rotation (10 h 39.4 min). Several recurrent spoke patterns have been observed at that period. Spoke activity showed a pronounced peak in the quadrant centered around 115°SLS (Saturn longitude system, defined by Desch and Kaiser 1981).

Spokes have been observed all around the illuminated side of the ring. However, they are visible with highest contrast relative to the underlying B ring at the morning ansa. Bright spokes were also observed on that face of the B ring, which is not illuminated by the sun, but illuminated only by Saturn's shine. From edge-on views of the ring system an upper limit of 80 km for the height of spokes above the ring plane is derived.

In the following discussion we briefly mention some of the theories on spoke formation which have been advanced and show their relation to the observations.

Several theories (Gold 1980, Bastin 1981, Carbary et al. 1982) propose that spokes become visible because elongated grains are aligned due to polarization in weak radial electric fields. But Weinheimer and Few (1982) have argued against grain alignment theories. They showed that grain alignment theories require that grains are sufficiently conducting. However, unless ice (spoke particles, like the rest of the ring par-

ticles, are most likely to be composed of H_2O-ice) becomes ferro-electric, the electric torque used to align the particles is many orders of magnitude too small with the electric fields expected in the B ring. Weinheimer and Few (1982) believe that it is very unlikely that the ice would become ferro-electric at the ring temperatures.

Most other theories proposed so far for spoke formation require charged dust particles which are elevated above the ring plane. Thomsen et al.(1982) interpret the deviation of the angular velocity of spoke features from the Keplerian value as being due to the orbital speed of negatively charged dust particles. The observed large deviations of the radial edge of active spokes (cf. Grün et al 1982) from Keplerian speed would be indicative in their model of very high negative charges ($|q/m| > 100$ Coul/kg) on dust particles.

Hill and Mendis (1981a, 1982a) discuss dust particle dynamics in their electromagnetic environment. They calculate the orbits of different-sized grains as they move around the planet and find that high negative charges on dust particles should give rise to fine structure in wedge-shaped spokes. They predict that a number of almost straight, sharp, "ribs", should radiate out from a point at the co-rotation distance, which revolve with time-varying angular speed. Finally they show that the resettling of the grains on the larger bodies in the ring plane following their initial levitation results in a differential transport of grains across the ring plane. A

consequence of this is the establishment of different multimodal size distributions of dust within the spokes at different planetocentric distances. All of these detailed predictions have not yet been uniquely verified by the observations.

The most comprehensive theories of spoke formation are those of Goertz and Morfill (1983) and Morfill et al. (1982c). Goertz and Morfill (1983) show that relatively dense plasma ($n \sim 100\ cm^{-3}$) is required near the rings in order to generate a strong enough surface electric field to lift dust particles off the ring. It is unlikely that the average plasma density near the rings is large enough to do this. Such a dense plasma cloud near the rings will contain slightly negatively charged dust which due to the gravitational force drifts relative to the plasma. This current causes a polarization of the plasma cloud and a radial $\underline{E} \times \underline{B}$ plasma drift with a speed of order of 30 km/s. As long as the drifting plasma is dense enough, dust will be elevated which marks the radial trail of the plasma.

The subsequent evolution of such a radially aligned negatively charged dust cloud is discussed by Morfill et al. (1982c). The discharge of the fine dust by solar UV radiation produces a cloud of electrons, which moves adiabatically in Saturn's dipolar magnetic field. The electron cloud is absorbed by the ring after one bounce, alters the local ring potential

significantly and reduces the local Debye length. As a result, more micron-sized dust particles may be elevated above the ring plane and the spoke grows in width. This process continues until the electron cloud has dissipated.

Both theories (Goertz and Morfill 1983, Morfill et al 1982c) are able to account for the energetics of spoke formation, dust levitation off the ring plane, radial alignment of young spokes, spoke formation times and the identification of structure (filamentary, narrow and extended spokes).

Open questions in these theories include the origin of the dense plasma clouds proposed by Goertz and Morfill (1983), and the cause for the periodicity of spoke activity. While there is no satisfying explanation for the spoke periodicity a number of proposals have been made for the origin of the dense plasma clouds. One possibility is meteoroid impacts (Morfill and Goertz, 1982, Morfill et al. 1982a); another is sputtering of the rings caused by field aligned currents of accelerated keV-particles (Morfill 1982b).

Acknowledgement

The authors are grateful to J.A. Burns for his helpful comments.

References

Acuña M A and Ness N F (1976)
Results from the GSFC fluxgate magnetometer on Pioneer 11.
In Jupiter (T. Gehrels, Ed) 830-847
Univ. of Arizona Press, Tucson

Acuña M H and Ness N F (1980)
The magnetic field of Saturn: Pioneer 11 observations
Science, 207, 444-446.

Ashworth D G (1978)
Lunar and planetary impact erosion
in Cosmic Dust (J A M McDonnell Ed) 427-526
Wiley Chichester, New York, Brisbare, Toronto

Bagenal F and Sullivan J D (1981)
Direct plasma measurements in the Io Torus and inner magnetosphere of Jupiter
J. Geophys. Res., 86, 8447-8466.

Barge P, Pellat R, Millet J (1982)
Diffusion of Keplerian motions by a stochastic force (I) A general formalisme
Astron. Astrophys., in press

Bastin J A (1981)
Note on the rings of Saturn,
The Moon and the Planets, 24, 467.

Belton M J S (1966)
Dynamics of interplanetary dust
Science, 151, 35-44.

Berg O E, Wolf H and Rhee J (1976)
Lunar soil movement registered by the Apollo 17 cosmic dust experiment,
in Interplanetary Dust and Zodiacal Light (H Elsässer and H. Fechtig Eds), 233-237, Springer-Verlag, Berlin

Bridge H S, Belcher J W, Lazarus A J, Sullivan J D, McNutt R L, Bagenal F, Scudder J D, Sittler E C, Siscoe G L, Vasyliunas V M, Goertz C K and Yeates C M (1979)
Plasma observation near Jupiter: Initial results from Voyager 1
Science, 204, 987-991.

Bridge H S, Belcher J W, Lazarus A J, Olbert S, Sullivan J D, Bagenal F, Gazis P R, Hartle R E, Ogilvie K W, Scudder J D, Sittler E C, Eviatar A, Siscoe G L, Goertz C K and Vasyliunas V M (1981)
Plasma Observations near Saturn: Initial results from Voyager 1.
Science, 212, 217-224.

Bridge H S, Bagenal F, Belcher J V, Lazarus A J, McNutt R L, Sullivan J D, Gazis P R, Hartle R E, Ogilvie K W, Scudder J D, Sittler E L, Eviatar A, Siscoe G L, Goertz C K and Vasyliunas V M (1982)
Plasma observations near Saturn: Initial results from Voyager 2.
Science, 215, 563-570.

Broadfoot A L, Sandel B R, Shemansky, D E, Holberg, J B, Smith G R, Strobel D F, McConnell J C, Kumar S, Hunten D M, Atreya S K, Donahue T M, Moos H W, Bertaux J L, Blamont J E, Pomphrey R B and Linick S (1981)
Extreme ultraviolet observations from Voyager 1 encounter with Saturn.
Science 212, 206-211.

Brown W L, Augustyniak W M, Brody E, Cooper B, Lanzerotti L J, Ramierez A, Evatt R and Johnson R E (1980)
Energy dependence of the erosion of H_2O ice films by H and He ions.
Nucl. Instrum. Method 170, 321-325.

Brown W L, Lanzerotti L J, Poate J M and Augustyaniak W M (1978)
Sputtering of ice by MeV light ions.
Phys. Rev. Lett. 40, 1027.

Burns J A, Lamy P L and Soter S (1979)
Radiation forces on small particles in the solar system.
Icarus 40, 1-48.

Burns J A, Showalter M R, Cuzzi J N and Pollack J B (1980)
Physical processes in Jupiter's ring: Clues to its origin by Jove!
Icarus 44, 339-360.

Burns J A, Showalter M R and Morfill G E (1982)
Jupiter's etheral ring.
This volume.

Carbary J F, Bythrow P F and Mitchell D G (1982)
The Spokes in Saturn's rings: A new approach.
Geophys. Res. Lett. 19, 420-422.

Carter G and Calligon J S (1968)
Ion Bombardment of Solids
Elsevier, New York

Ceplecha Z and Mc Crosky R E (1976)
Fireball end heights: a diagnostic for the structure of meteoric material.
J. Geophys. Res. 81, 6257.

Cheng A F, Lanzerotti L J and Pirronello V
Charged particle sputtering of ice surfaces in Saturn's magnetosphere.
J. Geophys. Res. 87, 4567-4570.

Connerney J E P, Ness N F and Acuna M H (1982).
Zonal harmonic model of Saturn's magnetic field from Voyager 1 and 2 observations.
Nature 298, 44-46.

Consolmagno G J (1980)
Electromagnetic scattering lifetimes for dust in Jupiter's ring.
Nature 285, 557-558.

Cuzzi J, Esposito L, Lissauer J
Physical properties of Saturn's ring.
This volume.

Davis D R, Housen K R and Greenberg R (1981).
The unusual dynamical environment of Phobos and Deimos.
Icarus 47, 220-223.

Dermott S F (1982)
Narrow rings.
This volume.

Dermott S F, Gold T and Sinclair A T (1979)
The rings of Uranus: Nature and origin.
Astron. J. 84, 1225-1234.

Dermott S F, Murray C D and Sinclair A T (1980)
The narrow rings of Jupiter, Saturn and Uranus.
Nature 284, 309-313.

Desch M D and Kaiser M L (1981)
Voyager measurement of the rotation period of Saturn's magnetic field.
Geophys. Res. Lett., 253-256.

Dobrovolskis A R and Burns J A (1980)
Life near the Roche limit: Behavior of ejecta from satellites close to planets.
Icarus 42, 422-441.

Dohnanyi J S (1969)
Collisional model of asteroids and their debris
J. Geophys. Res. 74, 2531-2554.

Durisen R H (1983).
Transport effects due to particle erosion mechanisms.
This volume.

Evans D R, Romig J H, Hord C W, Simmons K E, Warwick J W and Lane A L (1982).
The source of Saturn electric discharges.
Nature 299, 236-237.

Fechtig H, Grün E and Kissel J (1978)
Laboratory simulation.
In Cosmic Dust (J A M McDonnell Ed) 607-669,
Wiley, Chichester, New York, Brisbane, Toronto.

Fechtig H, Grün E and Morfill G E (1979).
Micrometeoroids within ten Earth radii.
Planet. Space Sci. 27, 511-531.

Feucherbacher B and Fitton B (1972)
Experimental investigation of photoemission from satellite surface materials.
J. Appl. Phys. 43, 1563-1572.

Fillius W (1976)
The trapped radiation belts of Jupiter.
In Jupiter (T. Gehrels Ed) pp. 896-927.
Univ. of Arizona Press, Tucson.

Fillius W, Ip W H and McIlwain C E (1980)
Trapped radiation belts of Saturn: First Look.
Science, 207, 425-431.

Frank L A, Ackerson K L, Wolfe J H and Milhalov J D (1976)
Observations of plasmas in the Jovian magnetosphere.
J. Geophys. Res. 81, 457-468.

Friichtenicht J F (1964)
Micrometeoroid simulation using nuclear accelerator techniques.
Nucl. Instrum. Meth. 28, 70-78.

Fujiwara A, Kamimoto G and Tsukamoto A (1977)
Destruction of basaltic bodies by high-velocity impact
Icarus 31, 277-288.

Gault D E and Heitowit E D (1963)
The partition of energy for hypervelocity impact craters formed in rock.
In Proceedings, Sixth Hypervelocity Impact Symposium, Vol. 2, pp. 419-456.

Gault D E, Hörz F and Hartung J B (1972)
Effects of microcratering on the lunar surface.
Proc. Third Lunar Conf. 3, 2713-2734.

Gault D E and Wedekind J A (1969)
The destruction of tektites by micrometeoroid impact.
J. Geophys. Res. 74, 6780-6794.

Goertz C K and Morfill G E (1983)
A model for the formation of spokes in Saturn's ring.
Icarus, 53, 219-229.

Goertz C K and Thomsen M F (1979)
The dynamics of the Jovian magnetosphere.
Rev. Geophys. and Space Physics 17, 731-743.

Gold T (1955)
Monthly Notices Roy Astron. Soc. 115, 585-604.

Gold T (1980)
Electric origin of the spokes seen in Saturn's rings.
Contribution to Royal Society Conf. On Planetary Exploration, London, Nov. 1980 (Transactions R.S.).

Grün E, Fechtig H and Kissel J (1983)
Physical and chemical characteristics of interplanetary dust: Measurements by Helios.
in preparation.

Grün E, Morfill G, Schwehm G and Johnson T V (1980)
A model of the origin of the Jovian ring
Icarus 44, 326-338.

Grün E, Morfill G E, Terrile R J, Johnson T V and Schwehm G (1982)
The evolution of spokes in Saturn's B ring.
Icarus, in press.

Gurnett D A, Grün E, Gallagher D, Kurth W S and Scarf F L (1983)
Micron-size particles detected near Saturn by the Voyager plasma wave instrument.
Icarus, 53, 236-254.

Haff P K, Watson C C and Tombrello T A (1979)
Ion erosion on the Galilean satellites of Jupiter.
Proc. Lunar Planet. Sci. Conf. 10, 1685-1699.

Hassan M, Wallis M K (1982)
Stochastic diffusion in inverse square field: General formulation for interplanetary gas.
Planet. Space Sci., in press.

Hill J.R and Mendis D.A. (1980)
Charged dust in the outer planetary magnetospheres
II Trajectories and spatial distribution
The Moon and the Planets, 23, 53-71.

Hill J R and Mendis D A (1981a)
On the braids and spokes in Saturn's ring system.
The Moon and the Planets, 24, 431-436.

Hill J R and Mendis D A (1981b)
Electrostatic disruption of a charged conducting spheroid
Can. J. of Physics 59, 897- 901

Hill J R and Mendis D A (1982a)
The dynamical evolution of the Saturnian ring spokes.
Geophys. Res. 87, 7413 - 7420.

Hill J R and Mendis D A (1982b)
The isolated non-circular ringlets of Saturn
The Moon and the Planets, 26, 217-226.

Hinteregger H E (1965)
Absolute intensity measurements in the extreme ultra-violet spectrum of solar radiation.
Space Sci. Rev. 4, 461-497.

Hoffman H, Fechtig H, Grün E und Kissel J (1975a)
First results of the micrometeoroid experiment S215 on HEOS 2 Satellite.
Planet. Space Sci. 23, 215-224.

Hoffmann H-J, Fechtig H, Grün und Kissel J (1975b)
Temporal fluctuations and anisotropy of the micrometeoroid flux in the earth-moon system.
Planet. Space Sci. 23, 985-991.

Hornung K and Drapatz S (1981)
Residual ionisation after impact of large dust particles.
in The Comet Halley Probe Plasma Environment, p. 23-37,
ESA SP-155.

Ip W-H (1982)
On plasma transport in the vicinity of the rings of Saturn:
A siphon flow mechanism.
J. Geophys. Res., in press.

Jewitt D C (1982).
The rings of Jupiter.
In: Satellites of Jupiter (D. Morrison, Ed.) pp. 44-64.
Univ. of Arizona Press, Tucson.

Jewitt D C and Danielson G E (1981)
The Jovian ring
J. Geophys. Res. 86, 8691-8697.

Johnson T V, Cook A F, Sagan C and Soderblom L A (1979)
Volcanic resurfacing rates and implications for volatiles on Io.
Nature 280, 746-750.

Johnson T V, Morfill G E and Grün E (1980)
Dust in Jupiter's magnetosphere: An Io source.
Geophys. Res. Lett. 7, 305-308.

Kaiser M L, Connerney J E P and Desch M D (1983).
The source of Saturn electrostatic discharges:
atmospheric storms.
NASA Technical Memorandum 84966, Goddard Space Flight
Center.

Krimigis S M, Armstrong T P, Axford W I, Bostrom C O, Gloeckler G,
Keath E P, Lanzerotti L J, Carbary J F, Hamilton D C and
Roelof E C (1981)
Low energy charged particles in Saturn's magnetosphere:
Results from Voyager 1.
Science 212, 225-231.

Krimigis S M, Armstrong T P, Axford W I, Bostrom C O, Gloeckler G,
Keath E P, Lanzerotti L J, Carbary J F, Hamilton D C and
Roelof E C (1982)
Low energy hot plasma and particles in Saturn's magnetosphere.
Science 215, 571-577.

Lange M A and Ahrens T J (1982)
Lunar and Planet.Science XIII, 415-416.

Lanzerotti J L, Brown W L, Poate J M and Augustyniak W M (1976)
On the contribution of water products from Galilean satellites to the Jovian magnetosphere.
Geophys. Res. Lett. 5, 155-158.

Matson D L, Johnson T V and Fanale F P (1974)
Sodium D-line emission from Io: Sputtering and resonant scattering hypothesis.
Astrophys. J. 192, L43-L46.

Mc Coy J E and Criswell D R (1974)
Evidence for a high altitude distribution of lunar dust.
Proc. Fifth Lunar Conf. 3, 2991-3005.

Mendis D A (1981)
The role of electrostatic charging of small and intermediate sized bodies in the solar system.
In: Investigating the Universe (F.D. Kahn, Ed.) 353-384.
D. Reidel Pub.Co., Dordrecht, Boston.

Mendis D A and Axford W I (1974)
Satellites and magnetospheres of the outer planets.
Ann. Rev. of Earth and Planet. Sci. 2, 419-474.

Mendis D A, Houpis H L F and Hill J R (1982a)
The gravito-electrodynamics of charged dust in planetary magnetospheres.
J. Geophys. Res. 87, 3449-3455.

Mendis D A, Houpis H L F and Hill J R (1982b)
Charged dust in Saturn's magnetosphere.
J. Geophys. Res. (Special Red Supplement of the XIIIth Lunar Planet. Sci. Conf., Houston, Texas, March 1982), in press

Meyer-Vernet N (1982)
"Flip-flop" of electric potential of dust grains in space, Astron.Astrophys. 105, 98-106.

Mignard F (1982)
Radiation effects.
This volume.

Morfill G E (1978)
A review of selected topics in magnetosphere physics.
Rep. Progr. Phys. 41, 303.

Morfill G E (1982a)
Electromagnetic effects in planetary rings.
Advances in Space Res., in press.

Morfill G E (1982b)
The formation of spokes in Saturn's rings.
Proc. of IAU Colloquium No. 75 on Planetary Rings, in press.

Morfill G E and Goertz C K (1982)
Plasma clouds in Saturn's rings.
Icarus, in press.

Morfill G E and Grün E (1979a)
The motion of charged dust particles in interplanetary space.
I. The zodiacal cloud
Planet. Space Sci. 27, 1269-1282.

Morfill G E and Grün E (1979b)
The motion of charged dust particles in interplanetary space
II. Interstellar grains.
Planet. Space Sci. 27, 1283-1292.

Morfill G E, Grün E and Johnson T V (1980a)
Dust in Jupiter's magnetosphere: Physical processes.
Planet. Space Sci. 28, 1087-1100.

Morfill G E, Grün E and Johnson T V (1980b)
Dust in Jupiter's magnetosphere: Origin of the ring.
Planet. Space Sci. 28, 1101-1110.

Morfill G E, Grün E and Johnson T V (1980c)
Dust in Jupiter's magnetosphere: Time variations.
Planet. Space Sci. 28, 1111-1114.

Morfill G E, Grün E and Johnson T V (1980d)
Dust in Jupiter's magnetosphere: Effect on magnetospheric electrons and ions.
Planet. Space Sci. 28, 1115-1123.

Morfill G E, Fechtig H, Grün E and Goertz C K (1982a)
Some consequences of meteoroid impacts on Saturn's ring.
Icarus, in press.

Morfill G E, Grün E, Johnson T V (1982b)
Saturn's E, G and F rings: Modulated by the plasma sheet.
J. Geophys. Res., in press.

Morfill G E, Grün E, Johnson T V and Goertz C K (1982c)
On the evolution of Saturn's spokes: Theory.
Icarus, in press.

Müller E W (1956)
Field desorption
Phys. Rev. 102, 618.

Mukai T (1980)
Grain disruption by collisions with the solar energetic particles.
In Solid Particles in the Solar System (I Halliday and B MacIntosh Eds) pp. 385-389, Reidel, Dordrecht.

Northrop T G (1963)
The adiabatic motion of charged particles.
John Wiley and Sons, New York.

Northrop T G and Hill J R (1982a)
On the adiabatic motion of charged dust grains in rotating magnetospheres.
J. Geophys. Res., in press.

Northrop T G and Hill J R (1982b)
Stability of negatively charged dust grains in Saturn's ring plane.
J.Geophys.Res. 87, 6045-6051.

Northrop T G and Hill J R (1983)
The inner edge of Saturn's B ring
J.Geophys.Res., in press.

Oechsner H (1975)
Sputtering - A review of some recent experimental and theoretical aspects.
Appl. Phys. 8, 185-198.

Öpik E J (1956)
Interplanetary dust and terrestrial accretion of meteoritic matter.
Irish Astron. J. 4, 84-135.

Owen T, Danielson G E, Cook A F, Hansen C, Hall V L and Duxbury T C (1979)
Jupiter's ring.
Nature 281, 442-446.

Peale S J (1966)
Dust belt of the Earth.
J. Geophys. Res. 71, 911-933.

Pollack J B, Burns J A and Tauber M E (1979)
Gas drag in primoridal circumplanetary envelopes: A mechanism for satellite capture.
Icarus 37, 587-611.

Porco C C and Danielson G E (1982)
The periodic variation of spokes in Saturn's rings.
Astronomical J 87, 826-833.

Rennilson J J and Criswell D R (1974)
Surveyor observations of lunar horizon-glow
The Moon 10, 121-142.

Rhee J W (1967)
Electrostatic potential of a cosmic dust particle.
In The Zodiacal Light and the Interplanetary Medium
(J C Weinberg Ed) 291-197, NASA SP-150.

Rhee J W (1976)
Electrostatic disruption of lunar dust particles.
In Interplanetary Dust and the Zodiacal Light
(H Elsässer and H Fechtig Eds) 238-240, Springer-Verlag, Berlin.

Scarf F L, Gurnett D A, Kurth W S and Poynter R L (1982)
Voyager plasma wave observations at Saturn.
Science 215, 287-294.

Schulz M (1975)
Geomagnetically trapped radiation.
Space Sci Rev. 17, 481-536.

Schulz M and Lanzerotti L J (1974)
Particle diffusion in the radiation belts.
Springer-Verlag, New York.

Scudder J D, Sittler Jr. E C and Bridge H S (1981)
A survey of the plasma electron environment of Jupiter: A view from Voyager.
J. Geophys. Res. 86, 8157-8179.

Severny A B, Terez E I and Zvereva A M (1974)
Preliminary results obtained with an astrophotometer installed on Lunokhod 2
Space Research XIV, 603-605.

Shapiro I I, Lautman D A and Colombo (1966)
The Earth's dust belt: Fact or fiction? 1. Forces perturbing dust particle motion.
J. Geophys. Res. 71, 5695-5704.

Showalter M R and Burns J A (1982)
A numerical study of Saturn's F ring
Icarus 52, 526-544.

Simpson J A, Bastian T S, Chenette D L, Lentz G A, Mc Kibben R B, Pyle K R and Tuzzolino A J (1980)
Saturnian trapped radiation and its absorption by satellites and rings: The first results from Pioneer 11.
Science 207, 411-415.

Singer S F and Walker E H (1962)
Photoelectric screening of bodies in interplanetary space.
Icarus 1, 7-12.

Sittler E C, Scudder J D and Bridge H S (1981)
Distribution of neutral gas and dust near Saturn.
Nature 292, 711-714.

Smith E J, Davis Jr. C, Jones D E, Coleman Jr. P J, Colburn D S, Dyal P and Sonett C P (1980)
Saturn's magnetic field and magnetosphere.
Science 207, 407-410.

Smith E J, Davis Jr. C, Jones D E, Coleman Jr. P J, Colburn D S, Dyal P, Sonett C P and Frandsen A M A (1974)
The planetary magnetic field and magnetosphere of Jupiter: Pioneer 10.
J. Geophys. Res. 79, 3501-3513.

Smith B A, Soderblom L, Beebe R, Boyce J, Briggs G, Bunker A, Collins S A, Hansen C J, Johnson T V, Mitchell J L, Terrile R J, Carr M, Cook II A F, Cuzzi J, Pollack J B, Danielson G E, Ingersoll A, Davies M E, Hunt G E, Masursky H, Shoemaker E, Morrison D, Owen T, Sagan C, Veverka J, Strom R and Suomi V E (1981)
Encounter with Saturn: Voyager 1 Imaging Science Results.
Science 212, 163-191.

Smith B A, Soderblom L, Batson R, Bridges P, Inge J, Masursky H, Shoemaker E, Beebe R, Boyce J, Briggs G, Bunker A, Collins S A, Hansen C J, Johnson T V, Mitchell J L, Terrile R J, Cook II A F, Cuzzi J, Pollack J B, Danielson G E, Ingersoll A, Davies M E, Hunt G E, Morrison D, Owen T, Sagan C, Veverka J, Strom R and Suomi V E (1982)
A new look at the Saturnian system: The Voyager 2 images.
Science 215, 504-537.

Smith B A, Soderblom L, Johnson T V, Ingersoll A, Collins S A, Shoemaker E M, Hunt G E, Carr M H, Davies M E, Cook II A F, Boyce J, Danielson G E, Owen T, Sagan C, Beebe R F, Veverka J, Strom R G, McCauley J F, Morrison D, Briggs G A and Suomi V E (1979)
The Jupiter system through the eyes of Voyager 1.
Science 204, 951-972.

Smoluchowski R (1989)
Existence and role of amorphous grains in the solar system.
In Solid Particles in the Solar System (I Halliday and B MacIntosh Eds), pp. 381-385, Reidel, Dordrecht.

Thomsen M F, Goertz C K, Northrop T G and Hill J R (1982)
On the nature of particles in Saturn's spokes.
Geophys. Res. Lett. 9, 423-426.

Van Allen J A (1977)
Distribution and dynamics of energetic particles in the Jovian magnetosphere.
Space Res. 17, 719-731.

Van Allen J A (1982)
Findings on rings and inner satellites of Saturn by Pioneer 11.
Icarus, 51, 509-527.

Van Allen J A, Thomsen M F, Randall B A, Rairden R L and Grosskreutz C L (1980a)
Saturn's magnetosphere, rings and inner satellites.
Science 207, 415-421.

Van Allen J A, Randall B A and Thomsen M F (1980b)
Sources and sinks of energetic electrons and protons in Saturn's magnetosphere.
J. Geophys. Res. 85, 5679-5694.

Van Allen J A, Thomsen M F and Randall B A (1980c)
The energetic charged particle absorption signature of Mimas.
J. Geophys. Res. 85, 5709-5718.

Vedder J F (1963)
Charging and acceleration of microparticles.
Rev. Sci. Instrum. 34, 1175-1183.

Vogt R E, Chenette D L, Cummings A C, Garrard T L, Stone E C, Schardt A W, Trainer J H, Lal N adn Mc Donald F B (1981)
Energetic charged particles in Saturn's magnetosphere: Voyager 1 results.
Science 212, 231-234.

Völk H J, Jones F C, Morfill G E and Röser S (1980)
Collisions between grains in a turbulent gas.
Astron. Astrophys. 85, 316-325.

Warwick J W, Pearce J B, Evans D R, Carr T D, Schauble J J, Alexander J K, Kaiser M L, Desch M D, Pedersen M, Lecacheux A, Daigne G, Boischot A and Barrow C H (1981)
Planetary radio astronomy observations from Voyager 1 near Saturn.
Science 212, 239-243.

Warwick J W, Evans D R, Romig J H, Alexander J K, Desch M D, Kaiser M L, Leblanc Y, Lecacheux A and Pedersen B M (1982)
Planetary radio astronomy observations from Voyager 2 near Saturn.
Science 215, 582-587.

Wechsung R (1977)
Industrial application of ion etching.
Proc. 7th Intern. Vac. Congr. and 3rd Intern. Conf. Solid Surfaces, 1237-1244.

Wehner G K, Kenknight C and Rosenberg D L (1963)
Sputtering rates under solar wind bombardment
Planet.Space Sci. 11, 885-895.

Weinheimer A J and Few A A (1982)
The spokes in Saturn's rings: A critical evaluation of possible electric processes.
Geophys.Res.Lett., 9, 1139-1142.

Wyatt S P (1969)
The electrostatic charge of interplanetary grains.
Planet.Space Sci. 17, 155-171.

FIGURE CAPTIONS

Figure 1: Plasma characteristics (density n and electron energy E_e) in the inner magnetosphere of Jupiter and Saturn. The plasma in the plasmasphere shows a systematic trend from high densities/low energies close to the planets (small L) to low densities/ high energies further away. Especially high densities are found in the Io torus and especially low plasma densities have been predicted above Saturn's A and B-ring. The dashed lines show the corresponding Debye length λ_D and the solid lines give the plasma electron fluxes. For comparison the photo electron flux from a metal surface is shown at the distances of Jupiter and Saturn.

Figure 2: Phase space density of energetic particles. For curve a no sources or sinks are assumed between L_o and L_4. For curve b a partially absorbing ring of particulates has been assumed between L_1 and L_3. The same "macro-signature" of the time averaged phase space density would be obtained from a satellite orbiting in the same distance interval. A time-dependent "micro-signature" (curve c) would be observed close to a satellite, or a clump of ring material.

Figure 3: Curves of constant τ ns as a function of ion (E_i) and electron (E_e) thermal energies. For plasma density n(cm^{-3})

and grain radius s(cm), τ is the time scale for charging up in seconds (from Johnson et al., 1980).

Figure 4: Maximum surface potentials for the electrostatic disruption of different materials which are characterized by their tensile strengths F_t. Electron field emission occurs at a surface field strength of $\sim 10^7$ V/cm. The line q = e indicates dust particles carrying only one electronic charge. Also shown are the limits of self-gravitation between a small particle with radius s_μ sitting on a large particle of radius s_o = 1.8 m and with the indicated surface potential for two charge states (number of electrons N) of the small particle: N = 1 and N = 700 $V_o s_\mu$ (free space charge).

Figure 5: Levitation and blow-off of small particles (radius s_μ) from a large particle (radius s_o). A surface potential V_o = 10 volts has been assumed and two charge states for the small particle: N = 1 and N = 700 $V_o s_\mu$. The Debye length was taken λ_D = 10 m. All small particles with radii left of the solid line will escape from the large particle. Particles with radii in between the solid and the broken lines will levitate and right of the broken line will stick to the surface of the large particles.

Figure 6: Pressure exerted on a dust grain by magnetospheric plasma. The effect of both direct collisions of ions (oxygen$^+$) and Coulomb collisions as a

function of relative velocity (in units of the speed of sound c_i) between plasma and grain. The electrostatic potential of the dust particle was taken V_o = 10 volts.

Figure 7: The variation of F_L/F_G (the ratio of the electric to the gravitational force) on grains of different sizes and different potentials V_o (Volts) within the Saturnian magnetosphere at L = 5.0 (a position within the broad E-ring). (From Mendis et al., 1982b).

Figure 8: The variation of ω_G with α (= ω_{Kep}/Ω). The curves marked A,B,C, D indicate the values of ω_G when $\omega^2 = 0$, for various values of α. The shaded regions are where $\omega^2 > 0$ and the unshaded regions are where $\omega^2 < 0$. The dark shading corresponds to negative particles while the light shading corresponds to positive grains. The lines marked $\omega_G = \pm\Omega\alpha$ represent large particles moving at Keplerian speed, while the dashed line marked $\omega_G = \Omega$ represents the co-rotating (small) particles. The values of α = 0.1, 0.7, 1 and 2.5 correspond to the limit of rigid corotation in in Saturn's magnetosphere, the F ring, the synchronous orbit, and Saturn's surface, respectively. (From Mendis et al., 1982a).

Figure 9: Division of the rotating plasmasphere by the dashed curves F = 0 into two plasma regimes according

to the consideration of the balance of the centrifugal and gravitational forces: (1) the upward siphon flow region denoted by the shaded area with equatorial distance $r \leq 1.6252\ R_s$; (2) the equatorial confinement region with $r > 1.6252\ R_s$ (from Ip 1982).

Figure 10: Dust particle diffusion in the inner Jovian magnetosphere. Diffusion coefficient due to charge fluctuations as a function of position in the inner magnetosphere. The plasma characteristics (n_i, E_e) used to derive this result are indicated. The contours are given for different values of $v^2 s^4$ (v = particle velocity, in cm/s, s = particle radius in cm) and the region of applicability of the guiding center diffusion theory is shown by the hatched lines (from Morfill et al., 1980a).

Figure 11: Radial dependence of equatorial dust particle density inside the orbit of Io. A mass loss rate of 12.8 g/sec from Io in the form of submicron sized particles ($\sim 10^{16}$ particles/sec) was assumed. Inside the Jovian ring at $\sim 1.8\ R_J$ the dust population increases by a factor $\sim$500 due to erosive collisions with parent bodies (from Morfill et al., 1980d).

Figure 12: Guiding center diffusion through charge fluctuations. Geometry of dust particle motion in the presence of charge fluctuations, which leads to guiding centre diffusion. x_i = distance from the gyrocenter

(indicated by roman numbers). Sudden changes in the charge occur at positions 1, 2 and 3.

Figure 13: Number of dust impacts onto the LEAM experiment per 3-hour period integrated over 22 lunar days (from Berg et al., 1976).

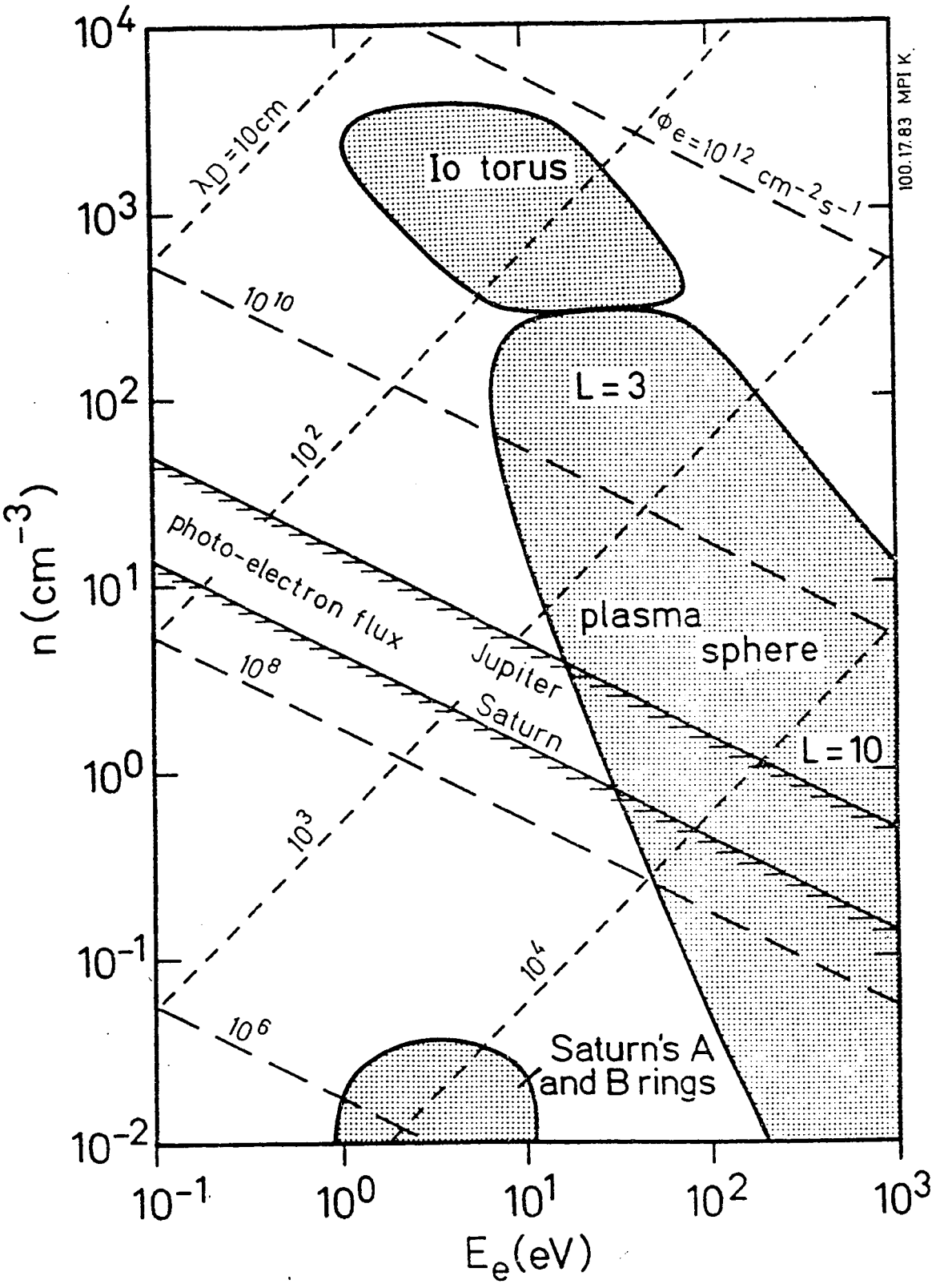
10^4
10^3
10^2
10^1
10^0
10^{-1}
10^{-2}
$n\,(cm^{-3})$
10^{-1}
10^0
10^1
10^2
10^3
$E_e(eV)$
$\lambda_D = 10cm$
$\Phi_e = 10^{12}\ cm^{-2}s^{-1}$
Io torus
10^{10}
L = 3
10^2
photo-electron flux
Jupiter
Saturn
plasma
sphere
10^8
L = 10
10^3
10^4
10^6
Saturn's A
and B rings
100.17.83 MPI K

Fig. 1

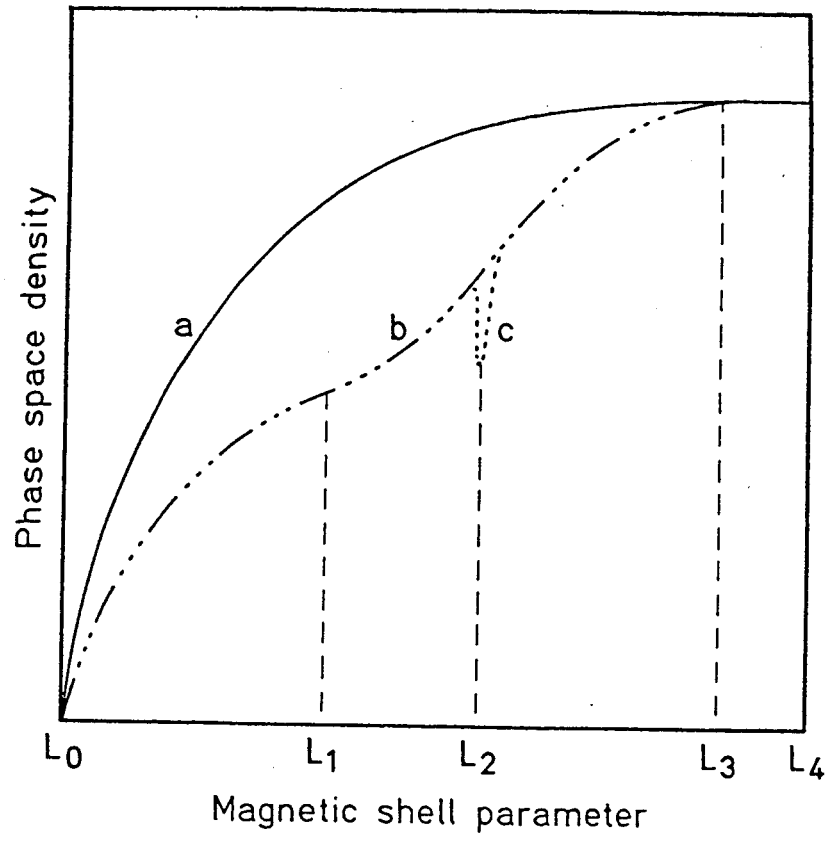
Phase space density
a
b
c
L_0
L_1
L_2
L_3
L_4
Magnetic shell parameter

Fig. 2.

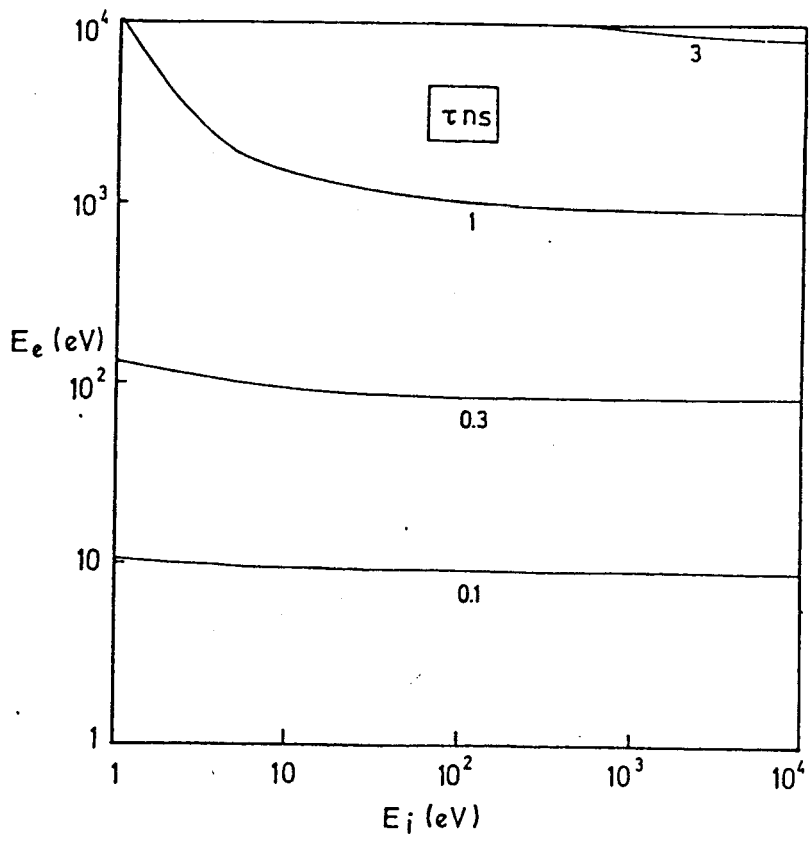
10^4
10^3
10^2
10
1
E_e (eV)
τns
3
1
0.3
0.1
1
10
10^2
10^3
10^4
E_i (eV)

Fig. 3.

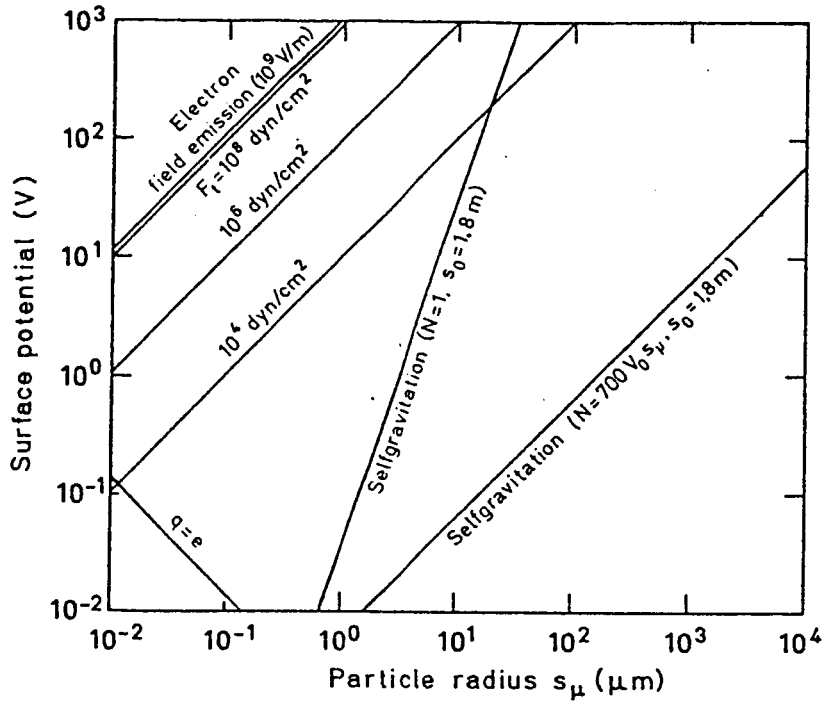
Surface potential (V)
Particle radius s_μ (μm)
Electron field emission (10^9 V/m)
$F_i = 10^8$ dyn/cm²
10^6 dyn/cm²
10^4 dyn/cm²
q = e
Selfgravitation (N=1, s_0=1,8 m)
Selfgravitation (N=700 $V_0 s_\mu$, s_0=1,8 m)

Fig. 4.

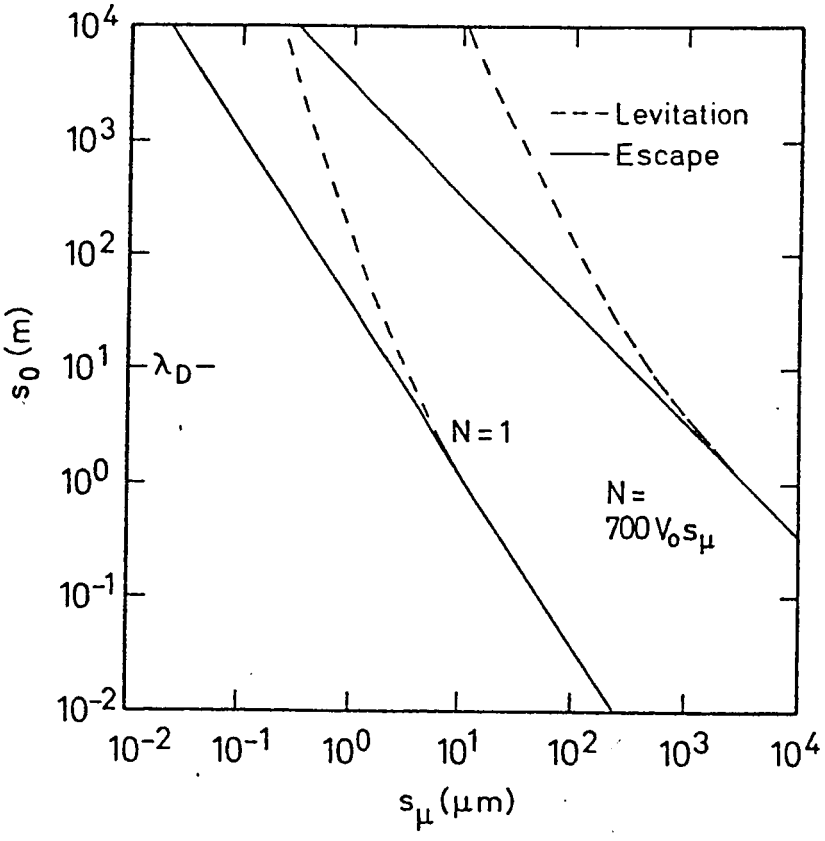
s_0 (m)
s_μ (μm)
Levitation
Escape
λ_D
N = 1
N = 700 $V_0 s_\mu$

Fig. 5.

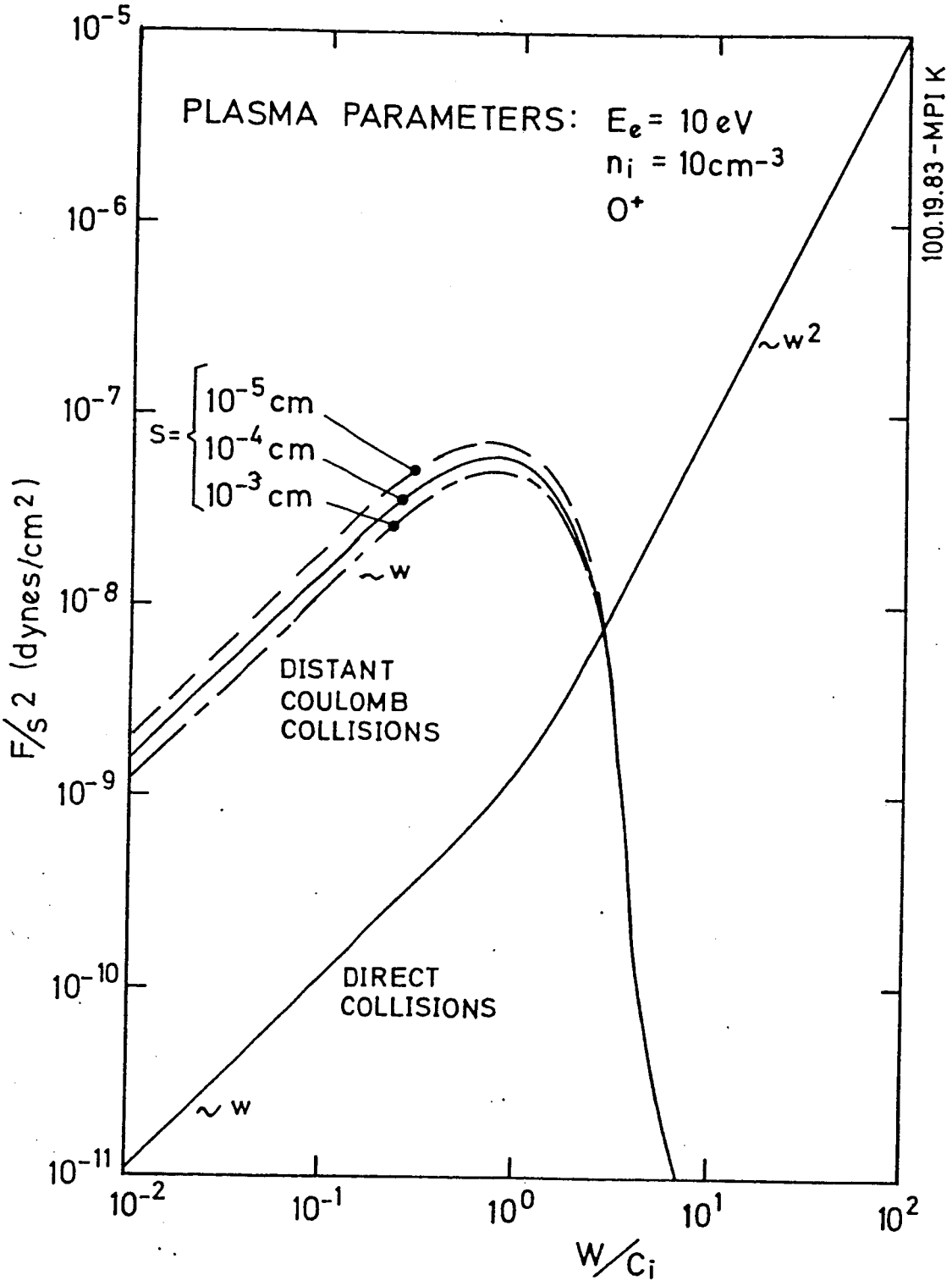
PLASMA PARAMETERS: E_e = 10 eV
n_i = 10cm^{-3}
O^+
100.19.83-MPI K
10^{-5}
10^{-6}
10^{-7}
10^{-8}
10^{-9}
10^{-10}
10^{-11}
F/S^2 (dynes/cm^2)
S= 10^{-5} cm
10^{-4} cm
10^{-3} cm
~w
~w^2
DISTANT
COULOMB
COLLISIONS
DIRECT
COLLISIONS
~ w
10^{-2}
10^{-1}
10^{0}
10^{1}
10^{2}
W/C_i

Fig. 6

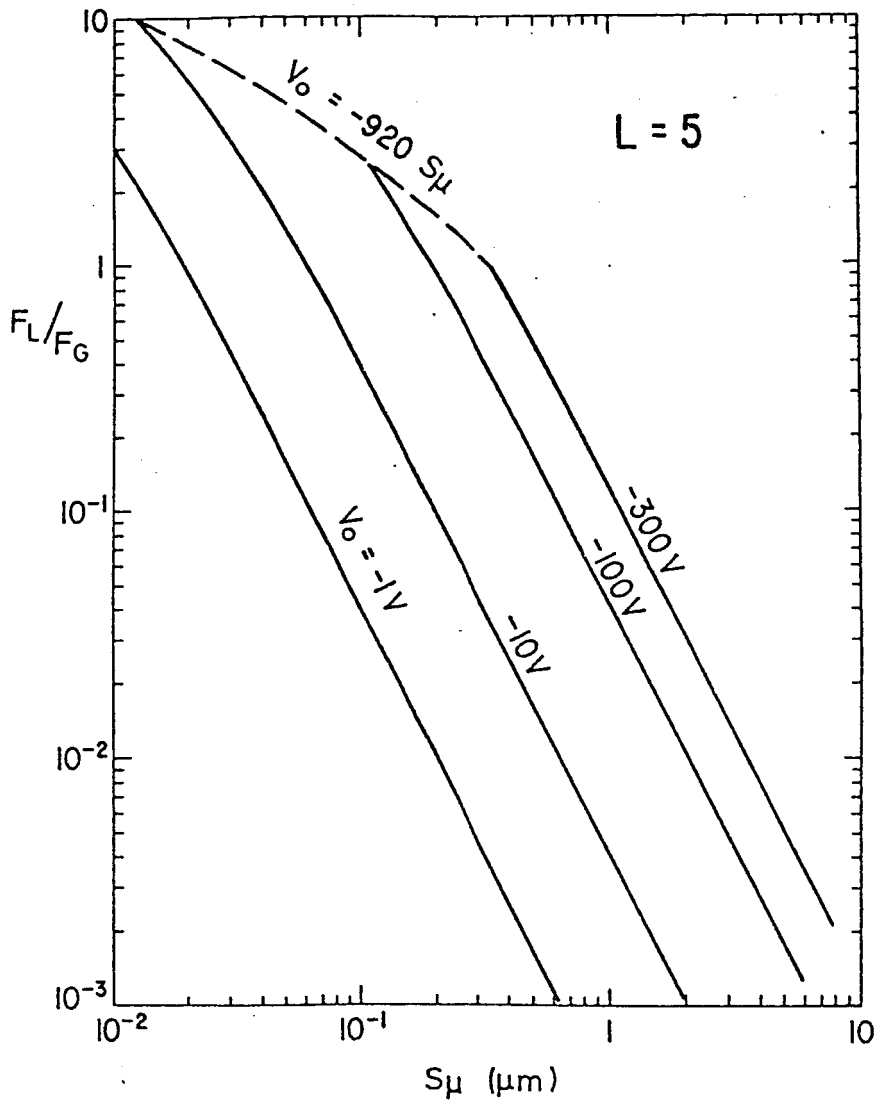
L = 5
V_o = -920 Sμ
-300V
-100V
-10V
V_o = -1V
F_L/F_G
Sμ (μm)
10
1
10^{-1}
10^{-2}
10^{-3}
10^{-2}
10^{-1}
1
10

Fig. 7.

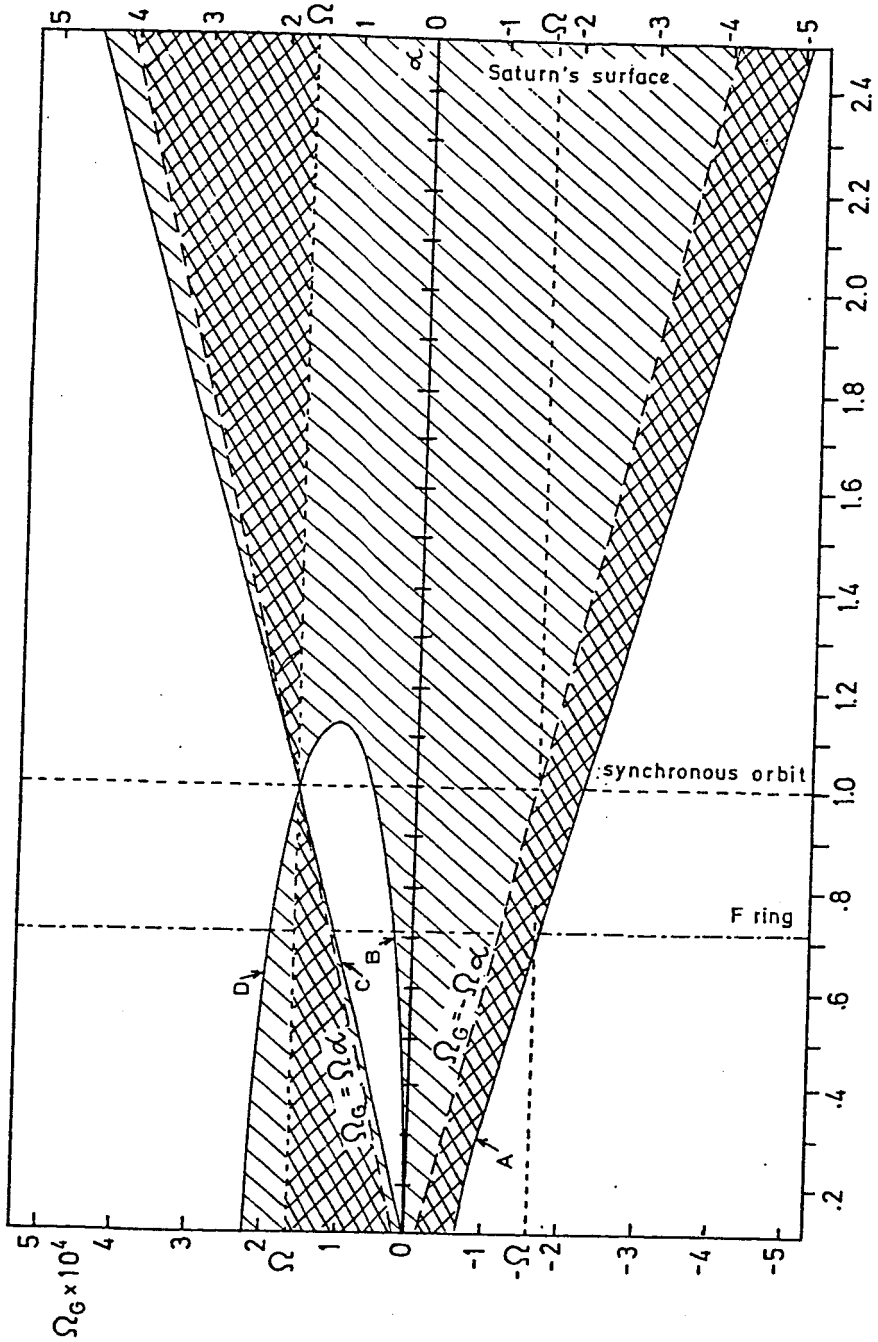
Saturn's surface
synchronous orbit
F ring
A
B
C
D
$\Omega_G = \Omega\alpha$
$\Omega_G = -\Omega\alpha$
$\Omega_G \times 10^4$
Ω
α

Fig. 8

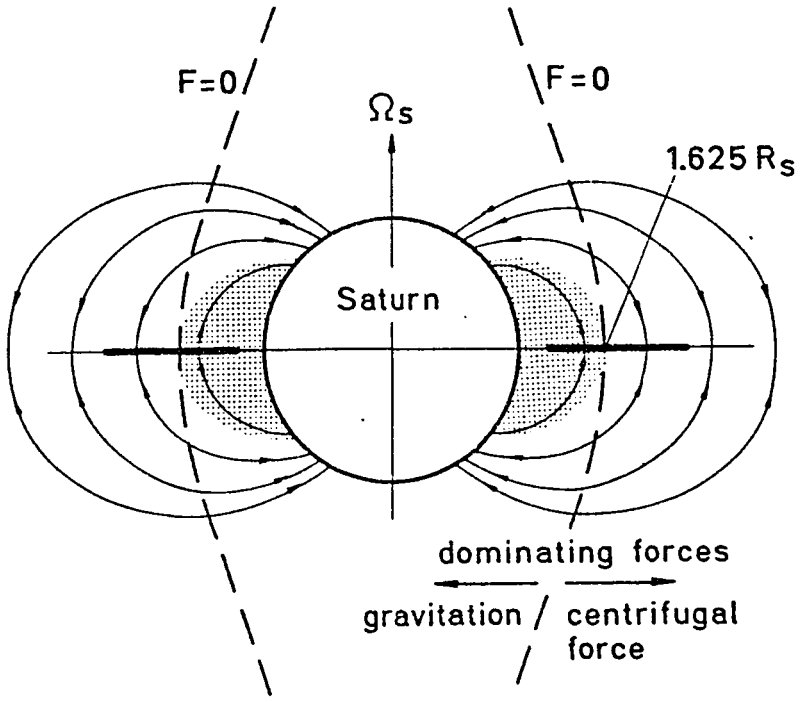
F=0
F=0
Ωs
1.625 Rs
Saturn
dominating forces
gravitation / centrifugal force

Fig. 9.

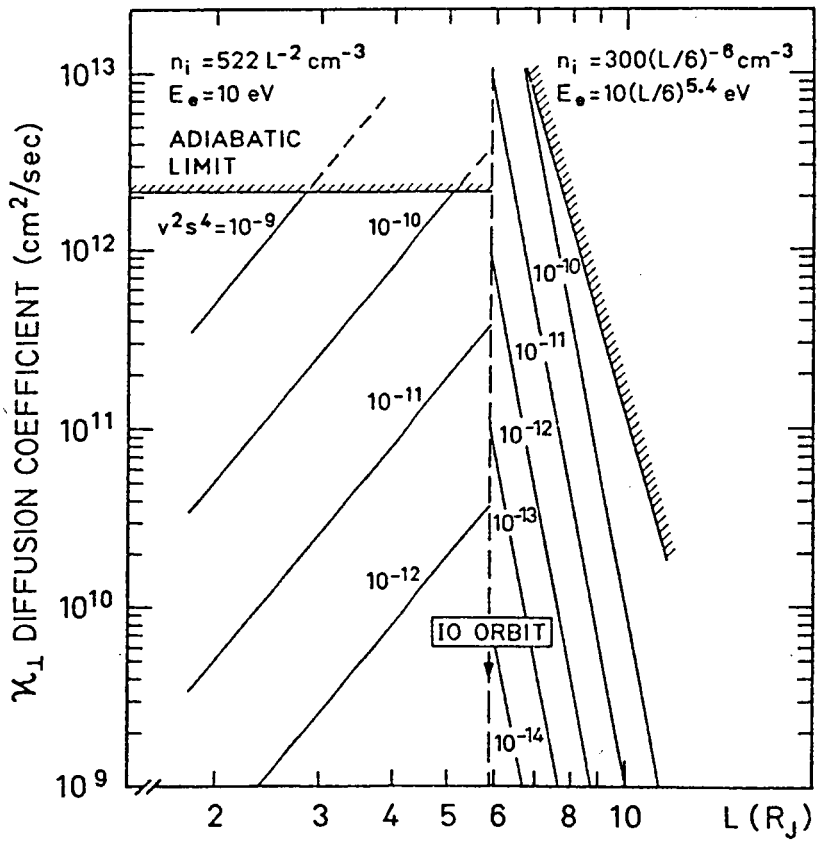
$n_i = 522\,L^{-2}\,cm^{-3}$
$E_e = 10$ eV
ADIABATIC LIMIT
$v^2 s^4 = 10^{-9}$
10^{-10}
10^{-11}
10^{-12}
$n_i = 300(L/6)^{-6}\,cm^{-3}$
$E_e = 10(L/6)^{5.4}$ eV
10^{-10}
10^{-11}
10^{-12}
10^{-13}
10^{-14}
IO ORBIT
$\chi_\perp$ DIFFUSION COEFFICIENT (cm^2/sec)
10^{13}
10^{12}
10^{11}
10^{10}
10^{9}
2
3
4
5
6
8
10
L (R_J)

Fig. 10.

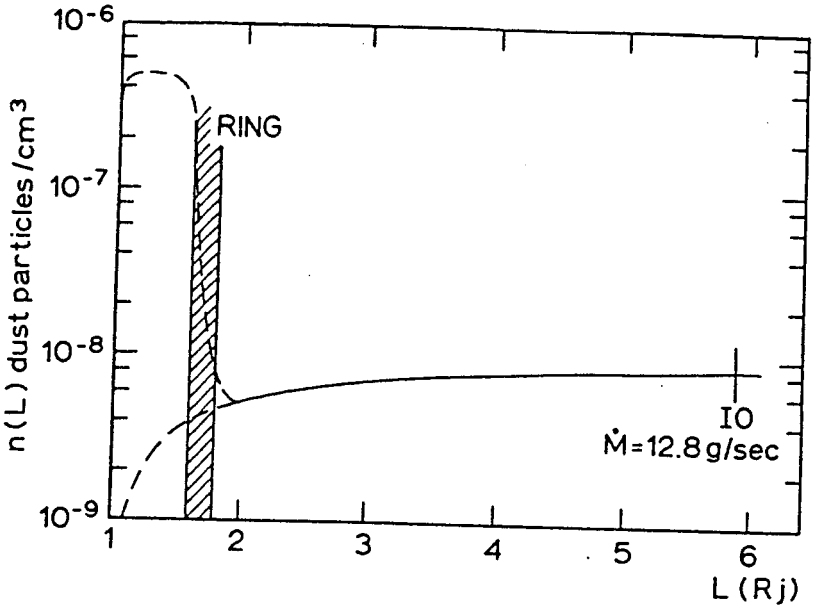

Fig. 11.

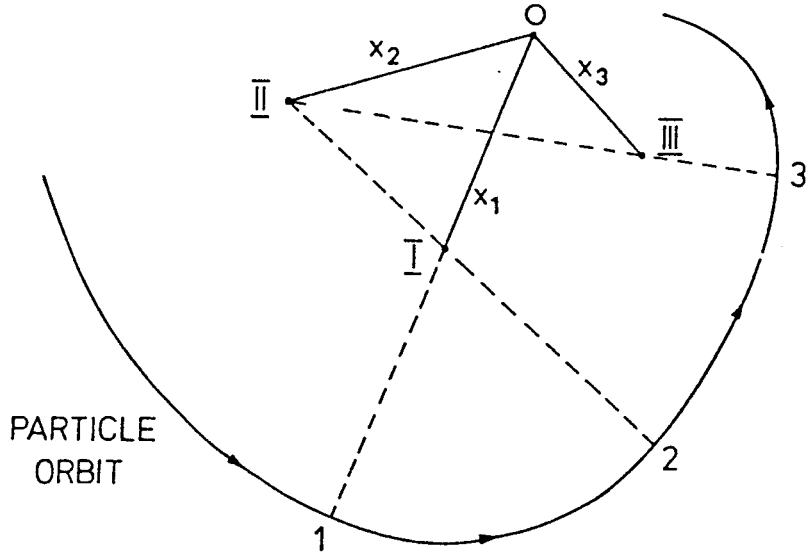

Fig. 12.

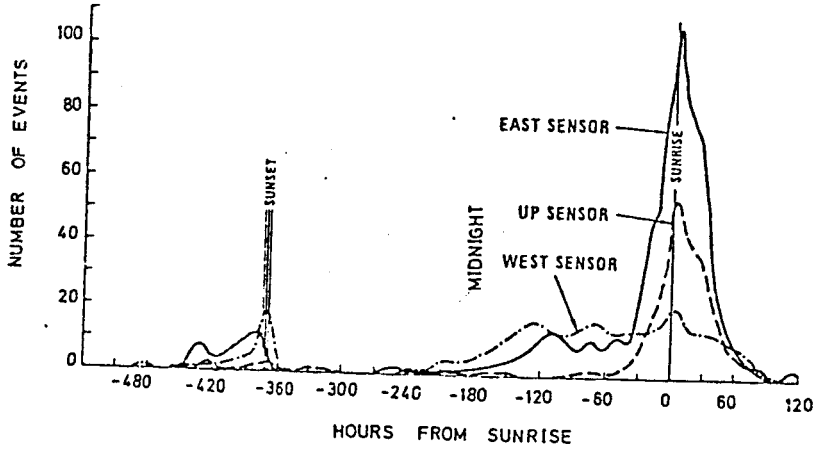

Fig. 13.